Electronic Supplementary Material (ESI) for Nanoscale.

Supporting Information

A gold-nanoparticle stoppered [2]rotaxane

Anne Ulfkjær,[†] Frederik W. Nielsen,[†] Hana Al-Kerdi,[†] Tamara Ruß,[†] Zaki K. Nielsen,[†] Jens Ulstrup,[‡] Lanlan Sun,[§] Kasper Moth-Poulsen,*[,§] Jingdong Zhang,*[,‡] Michael Pittelkow.*[,†]

[†] Department of Chemistry, University of Copenhagen, Universitetsparken 5, DK-2100 Copenhagen, Denmark

[‡] Department of Chemistry, Technical University of Denmark, Kemitorvet, Building 207, DK-2800 Kongens Lyngby, Denmark

[§] Department of Chemical and Biological Engineering, Chalmers University of Technology, Kemivägen 4, SE-41296 Gothenburg, Sweden

Contents

S1. Synthetic experimental procedures

S1.1. General methods

All chemicals, unless otherwise stated, were purchased from commercial suppliers and used as received. All solvents were high-performance liquid chromatography (HPLC) grade, except solvents used for dry column vacuum chromatography, which were technical grade. Hexane was dried by standing over molecular sieves (4 Å) for at least 5 days prior to use. Solvents were degassed by bubbling N_2 through the solvent, while ultrasonicated for 20 minutes. All reactions were carried out under an anhydrous nitrogen atmosphere unless otherwise stated.

Analytical thin layer chromatography (TLC) was performed on Merck SiO_2 60 F_{254} TLC plates or Merck neutral Al_2O_3 60 F_{254} TLC plates. Dry column vacuum chromatography was performed using SiO_2 from ROCC (SI 1722, 60 Å, 15–40 μm) or neutral Al_2O_3 from Riedel-De Haën AG (< 30 μm). Melting points (mp.) were determined on a Büchi melting point apparatus and are uncorrected.

^{1}H nuclear magnetic resonance spectroscopy (NMR) and ^{13}C NMR spectra were recorded at 500 MHz and 125 MHz, respectively, on a Bruker Ultrashield Plus 500 spectrometer using residual non-deuterated solvent as the internal standard. All chemical shifts (δ) are quoted in ppm and all coupling constants (J) are expressed in Hertz (Hz). The following abbreviations are used for convenience in reporting the multiplicity for NMR resonances: s = singlet, bs = broad singlet, d = doublet, t = triplet, q = quartet, and m = multiplet. Samples were prepared using $CDCl_3$ or D_2O purchased from Euriso-Top, DMSO-d_6 purchased from Cambridge Isotope Labs, or DCl purchased from Sigma Aldrich. The NMR data was processed using MestReNova v. 8.1.2. Assignment of all ^{1}H and ^{13}C resonances was achieved using standard 2D NMR techniques as ^{1}H-^{1}H COSY, ^{1}H-^{13}C HSQC, and ^{1}H-^{13}C HMBC.

HPLC analysis was performed on a Dionex UltiMate 3000 system coupled to an UltiMate 3000 diode array UV/Vis detector. Separations were achieved using a Dionex Acclaim RSLC 120 C18 2.2 μm 120 Å 2.1 × 100 mm column maintained at 20 °C. The mobile phase solutions prepared with 0.1 % HCOOH in the solvents. The water used as eluent was purified by a Millipore system. LC/MS was carried out on a Bruker MicrOTOF-QII-system with ESI-source with nebulizer 1.2 bar, dry gas 8.0 L min^{-1}, dry temperature 200 °C, capillary −4500 V, end plate offset −500 V, funnel 1 RF 200.0 Vpp, ISCID energy 0.0 eV, funnel 2 RF 200.0 Vpp, hexapole RF 100.0 Vpp, quadrupole ion energy 5.0 eV, low mass 100.00 *m*/*z*, collision energy 8.0 eV, collision RF 100.0 Vpp, transfer time 80.0 μs, and pre puls storage 1.0 μs. LC/HRMS samples were calibrated by an automated pre-run internal mass scale calibration of the individual samples by injecting a sodium formate solution, consisting of 10 mM $NaOH_{(aq)}$ in *i*-PrOH:H_2O 1:1 v/v (+ 1 % HCOOH). Subsequent calibration was performed based on the calibrator ions. The LC/MS data was processed using DataAnalysis v. 4.0 SP 5. For Br-containing ions in the mass spectrum, only the main bromine isotope (^{79}Br) is quoted.

Gas chromatography–mass spectrometry (GC-MS) was carried out using an Agilent 6890 series GC-system, with an Agilent 5973 Network Mass Selective detector, an Agilent 7683 series injector and an Agilent 7683 auto sampler. GC-MS data were processed using Enhanced Data Analysis v. E.01.00.237.

Elemental analysis was performed by the microanalytically service of the Department of Chemistry, University of Copenhagen, Denmark on a CE Instrument (Flash 1112 series EA).

S1.2. Procedures

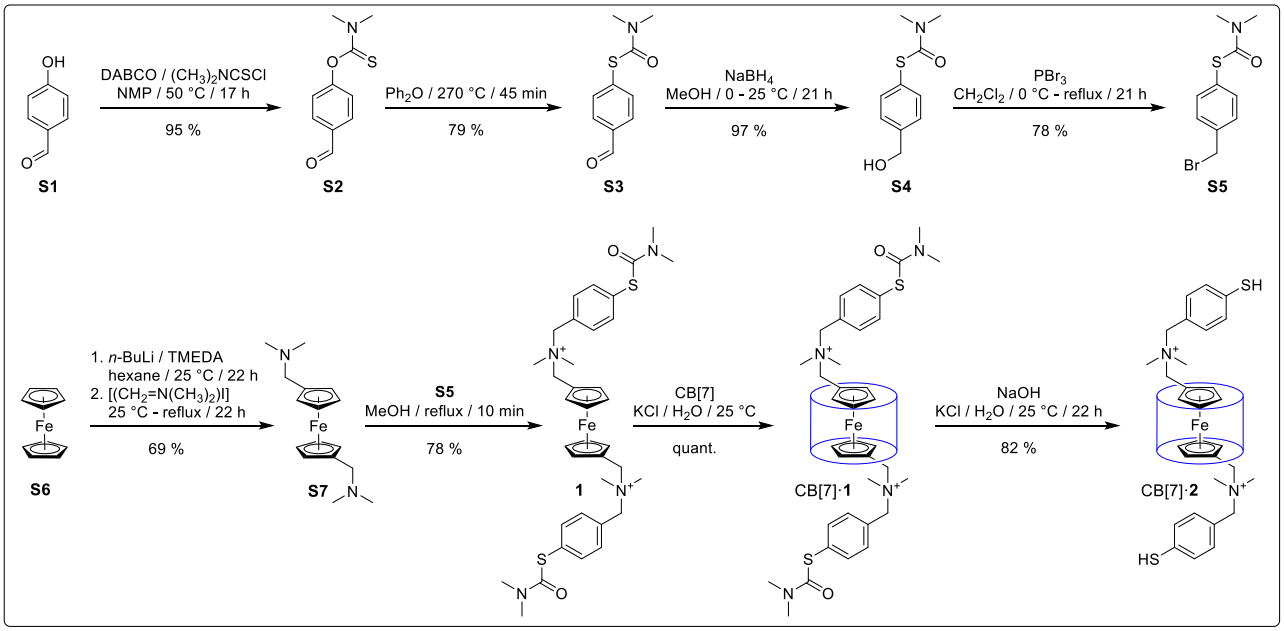

Scheme S1 Synthetic pathway for **1**, CB[7]·**1**, and CB[7]·**2**.

O-(4-Formylphenyl) *N*,*N*-dimethylthiocarbamate (S2)

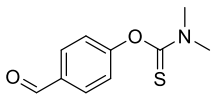

4-Hydroxybenzaldehyde (**S1**; 10.0 g, 81.9 mmol) and DABCO (11.9 g, 106 mmol) were suspended in NMP (50 mL) and heated to 50 °C. To this clear reaction mixture *N*,*N*-dimethylthiocarbamoyl chloride (11.1 g, 90.1 mmol), dissolved in NMP (20 mL), was added dropwise and the reaction mixture became turbid. The reaction mixture was hereafter left standing at 50 °C for 17 hours before cooled down to 25 °C. After this, H_2O (150 mL) was added dropwise and the initial solid dissolved readily, before a precipitate formed halfway through the addition which persisted to the end. The suspension was cooled to 5 °C overnight and the precipitate was isolated by filtration and washed with H_2O. The crude product was further purified by recrystallisation from MeOH/H_2O to yield the title compound as a white crystalline solid (16.3 g, 78.0 mmol, 95 %), mp. 93–94 °C. ^{1}H NMR (500 MHz, $CDCl_3$, 298 K): δ = 10.01 (s, 1H), 7.93 (d, J = 8.5 Hz, 2H), 7.25 (d, J = 8.5 Hz, 2H), 3.47 (s, 3H), 3.37 (s, 3H). ^{13}C NMR (125 MHz, $CDCl_3$, 298 K): δ = 191.09, 186.85, 158.64, 134.18, 131.08, 123.89, 43.48, 39.07. LC/HRMS: m/z = 210.0579 $[M+H]^+$ (calculated 210.0583). Elemental analysis (%) found (calculated) for $C_{10}H_{11}NO_2S$: C 57.40 (57.40), H 5.47 (5.30), N 6.72 (6.69).

S-(4-Formylphenyl) *N*,*N*-dimethylthiocarbamate (S3)

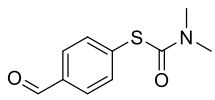

O-(4-Formylphenyl) *N*,*N*-dimethylthiocarbamate (**S2**; 14.0 g, 66.9 mmol) was dissolved in anhydrous Ph_2O (125 mL) and heated to 270 °C for 45 minutes. The reaction mixture was hereafter cooled to 25 °C, diluted with petroleum ether and directly subjected to dry column vacuum chromatography (SiO_2, three fractions with 100 % petroleum ether, then petroleum ether to CH_2Cl_2 with 20 % gradient, and then to 25 % EtOAc with 5 % gradient). The desired *S*-(4-formylphenyl) *N*,*N*-dimethylthiocarbamate (**S3**) was isolated as a light yellow crystalline solid (11.1 g, 53.0 mmol, 79 %), mp. 67–68 °C. ^{1}H NMR (500 MHz, $CDCl_3$, 298 K): δ = 10.03 (s, 1H), 7.87 (d, J = 8.2 Hz, 2H), 7.68 (d, J = 8.2 Hz, 2H), 3.11 (s,

3H), 3.05 (s, 3H). ^{13}C NMR (125 MHz, $CDCl_3$, 298 K): δ = 191.74, 165.47, 136.84, 136.34, 135.72, 129.85, 37.16, 37.11. LC/HRMS: *m/z* = 210.0586 $[M+H]^+$ (calculated 210.0583). Elemental analysis (%) found (calculated) for $C_{10}H_{11}NO_2S$: C 57.50 (57.40), H 5.26 (5.30), N 6.76 (6.69).

_S_-(4-(Hydroxymethyl)phenyl) _N_,_N_-dimethylthiocarbamate (S4)

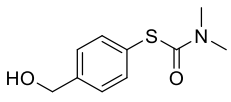

S-(4-Formylphenyl) *N*,*N*-dimethylthiocarbamate (**S3**; 4.56 g, 21.8 mmol) was dissolved in MeOH (110 mL) and cooled to 0 °C before $NaBH_4$ (905 mg, 23.9 mmol) was added slowly. The reaction mixture was hereafter stirred at 0 °C for 1 hour and then 20 hours at 25 °C. The reaction mixture was concentrated *in vacuo* and then redissolved in CH_2Cl_2 (110 mL) before H_2O (80 mL) was added and pH adjusted to ~ 1 with 2 M HCl (18 mL). The aqueous phase was extracted with CH_2Cl_2 (50 mL) and the combined organic phase was dried (Na_2SO_4), filtered, and concentrated *in vacuo* to yield the title compound as a light yellow crystalline solid (4.46 g, 21.1 mmol, 97 %), mp. 70–71 °C. ^{1}H NMR (500 MHz, $CDCl_3$, 298 K): δ = 7.48 (d, *J* = 8.2 Hz, 2H), 7.38 (d, *J* = 8.2 Hz, 2H), 4.70 (d, *J* = 4.8 Hz, 2H), 3.09 (s, 3H), 3.03 (s, 3H), 1.72 (t, *J* = 4.8 Hz, 1H). ^{13}C NMR (125 MHz, $CDCl_3$, 298 K): δ = 167.09, 142.22, 136.05, 127.99, 127.45, 65.02, 37.07. LC/HRMS: *m/z* = 212.0741 $[M+H]^+$ (calculated 212.0740). Elemental analysis (%) found (calculated) for $C_{10}H_{13}NO_2S$: C 56.69 (56.85), H 6.25 (6.20), N 6.56 (6.63).

_S_-(4-(Bromomethyl)phenyl) _N_,_N_-dimethylthiocarbamate (S5)

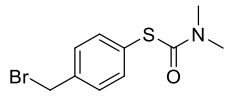

S-(4-(Hydroxymethyl)phenyl) *N*,*N*-dimethylcarbamothioate (**S4**; 1.04 g, 4.92 mmol) was dissolved in CH_2Cl_2 (12 mL) and cooled to 0 °C before PBr_3 (2.81 mL, 8.02 g, 29.6 mmol) was added dropwise. The reaction mixture was hereafter kept at 0 °C for 1 hour and then refluxed for 20 hours. After this, the mixture was cooled to 25 °C and poured into H_2O (20 mL). The organic phase was separated, dried (Na_2SO_4), filtered, and concentrated *in vacuo* to give *S*-(4-(bromomethyl)phenyl) *N*,*N*-dimethylcarbamothioate (**S5**) as a pale yellow crystalline solid (1.05 g, 3.83 mmol, 78 %), mp. 99–100 °C. ^{1}H NMR (500 MHz, $CDCl_3$, 298 K): δ = 7.47 (d, *J* = 8.2 Hz, 2H), 7.40 (d, *J* = 8.2 Hz, 2H), 4.48 (s, 2H), 3.06 (bs, 6H). ^{13}C NMR (125 MHz, $CDCl_3$, 298 K): δ = 166.64, 138.83, 136.06, 129.65, 129.24, 37.07, 32.82. LC/HRMS: *m/z* = 273.9902 $[M+H]^+$ (calculated 273.9896). Elemental analysis (%) found (calculated) for $C_{10}H_{12}BrNOS$: C 43.86 (43.81), H 4.26 (4.41), N 5.02 (5.11).

1,1'-Bis(_N_,_N_-dimethylaminomethyl)ferrocene (S7)[1]

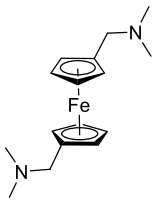

In a flame dried flask under a nitrogen atmosphere *n*-BuLi (1.11 M in hexane, 22.3 mL, 1.58 g, 24.7 mmol) was added dropwise to a solution of ferrocene (2.00 g, 10.8 mmol) and *N*,*N*,*N*',*N*'-tetramethylethane-1,2-diamine (TMEDA; 3.70 mL, 2.87 g, 24.7 mmol) in anhydrous hexane (100 mL). The reaction mixture was then stirred at 25 °C for 22 hours before it was diluted with anhydrous Et_2O (100 mL). *N,N*-Dimethylmethyleneiminium iodide (4.57 g, 24.7 mmol) was subsequently added and the resulting mixture was stirred at 25 °C for 22 hours. Afterwards, it was heated to reflux for 10 minutes and then cooled to 25 °C before H_2O (20 mL) was added dropwise to quench the reaction. After stirring for 10 minutes another portion of water (40 mL) was added. The phases were separated and the aqueous phase was extracted with Et_2O (3 × 100 mL) and the combined organic phase was washed with H_2O (100 mL), dried (Na_2SO_4), and concentrated *in vacuo*. The crude product was purified by dry column vacuum chromatography (neutral Al_2O_3, heptane to 30 % Et_2O with 5 % gradient, then one fraction of 100 % Et_2O, and then to 10 % MeOH with 1 % gradient) to yield **S7** as a brown oil (2.21 g, 7.37 mmol, 69 %). ^{1}H NMR (500 MHz, $CDCl_3$, 298 K): δ = 4.07 (d, *J* = 1.6 Hz, 4H), 4.04 (d, *J* = 1.6 Hz, 4H), 3.23 (s, 4H), 2.14 (s, 12H). ^{13}C NMR (125 MHz, $CDCl_3$, 298 K): δ = 83.58, 70.70, 68.73, 59.16, 44.89. LC/HRMS: *m/z* = 301.1357 $[M+H]^+$

(calculated 301.1362). Elemental analysis (%) found (calculated) for $C_{16}H_{24}FeNO_2$: C 64.04 (64.01), H 8.12 (8.06), N 9.21 (9.33).

Compound 1

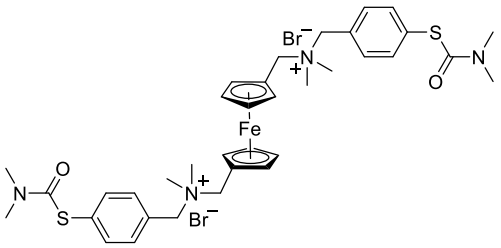

S-(4-(Bromomethyl)phenyl) *N*,*N*-dimethylcarbamothioate (**S5**; 1.63 g, 5.94 mmol) was added to a solution of 1,1'-bis(*N*,*N*-dimethylaminomethyl)ferrocene (**S7**; 600 mg, 2.00 mmol) in MeOH (25 mL) and the mixture was heated to reflux for 10 minutes. After cooling to 0 °C, Et_2O (150 mL), also cooled to 0 °C, was added and a precipitate formed. The solid was isolated by centrifugation and recrystallised from MeOH/Et_2O to obtain the desired product as a sandy coloured solid (1.33 g, 1.56 mmol, 78 %), mp. 105–107 °C. ^{1}H NMR (500 MHz, 100 mM KCl in D_2O, 298 K): δ = 7.67 (d, J = 8.0 Hz, 4H), 7.61 (d, J = 8.0 Hz, 4H), 4.68 (d, J = 1.9 Hz, 4H), 4.59 (d, J = 1.9 Hz, 4H), 4.53 (s, 4H), 4.49 (s, 4H), 3.17 (s, 6H), 3.02 (s, 6H), 2.91 (s, 12H). ^{13}C NMR (125 MHz, 100 mM KCl in D_2O added a DMSO lock tube, 298 K): δ = 168.32, 135.31, 132.67, 130.08, 127.79, 72.59, 72.48, 71.08, 66.02, 64.59, 47.41, 36.06, 35.83. LC/HRMS: m/z = 344.1281 $[M–2Br]^{2+}$ (calculated 344.1279). Elemental analysis (%) found (calculated) for $C_{36}H_{48}Br_2FeN_4O_2S_2$: C 50.92 (50.96), H 5.79 (5.70), N 6.33 (6.60).

Complex CB[7]·1

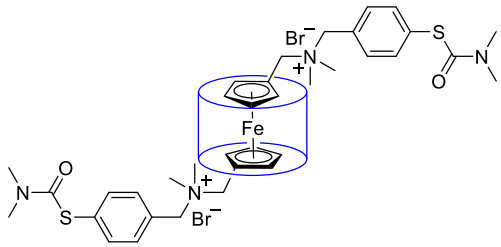

Equimolar amounts of compound **1** (4.24 mg, 5.00 µmol) and cucurbit[7]uril (CB[7]; 5.81 mg, 5.00 µmol) were mixed in D_2O (500 µL) containing 100 mM KCl at 25 °C. From the resulting clear, colourless solution containing inclusion complex CB[7]·**1** analytical data was recorded. ^{1}H NMR (500 MHz, 100 mM KCl in D_2O, 298 K): δ = 7.75 (d, J = 8.1 Hz, 4H), 7.68 (d, J = 8.1 Hz, 4H), 5.84 (d, J = 15.4 Hz, 14H), 5.64 (s, 14H), 4.41 (s, 4H), 4.34 (d, J = 15.4 Hz, 14H), 4.00 (s, 4H), 3.98 (d, J = 1.9 Hz, 4H), 3.82 (d, J = 1.9 Hz, 4H), 3.18 (s, 6H), 3.03 (s, 6H), 2.91 (s, 12H). ^{13}C NMR (125 MHz, 100 mM KCl in D_2O added a DMSO lock tube, 298 K): δ = 168.56, 155.50, 135.18, 132.99, 129.50, 128.71, 72.07, 71.86, 70.37, 69.35, 66.07, 65.06, 51.73, 47.52, 36.09, 35.83. LC/HRMS: m/z = 925.3011 $[M–2Br]^{2+}$ (calculated 925.2998).

Complex CB[7]·2

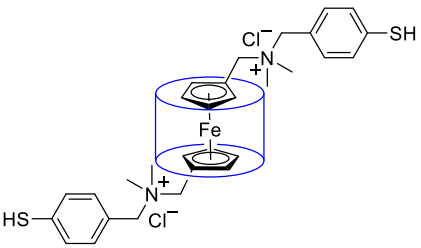

Equimolar amounts of compound **1** (100 mg, 118 µmol) and cucurbit[7]uril (CB[7]; 137 mg, 118 µmol) were suspended in a 2 M NaOH solution (40 mL) containing 100 mM KCl, which was degassed (N_2, 15 minutes) prior to use. The reaction mixture was left stirring at 25 °C for 22 hours before the suspension was centrifuged. The resulting solid was washed with H_2O (2 × 40 mL) and dried with Et_2O (40 mL) to obtain inclusion complex CB[7]·**2** as a light sandy coloured solid (136 mg, 96.8 µmol, 82 %), mp. > 250 °C. ^{1}H NMR (500 MHz, 100 mM KCl in 4 M DCl, 298 K): δ = 6.59 (d, J = 8.2 Hz, 4H), 6.55 (d, J = 8.2 Hz, 4H), 4.44 (d, J = 15.3 Hz, 14H), 4.38 (s, 14H), 3.12 – 3.05 (m, 18H), 2.65 (s, 4H), 2.61 (s, 4H), 2.45 (s, 4H), 1.53 (s, 12H). LC/HRMS: m/z = 854.2628 $[M–2Cl]^{2+}$ (calculated 854.2626).

S2. NMR characterisation of inclusion complexes

S2.1. Comparison of ^{1}H NMR spectra

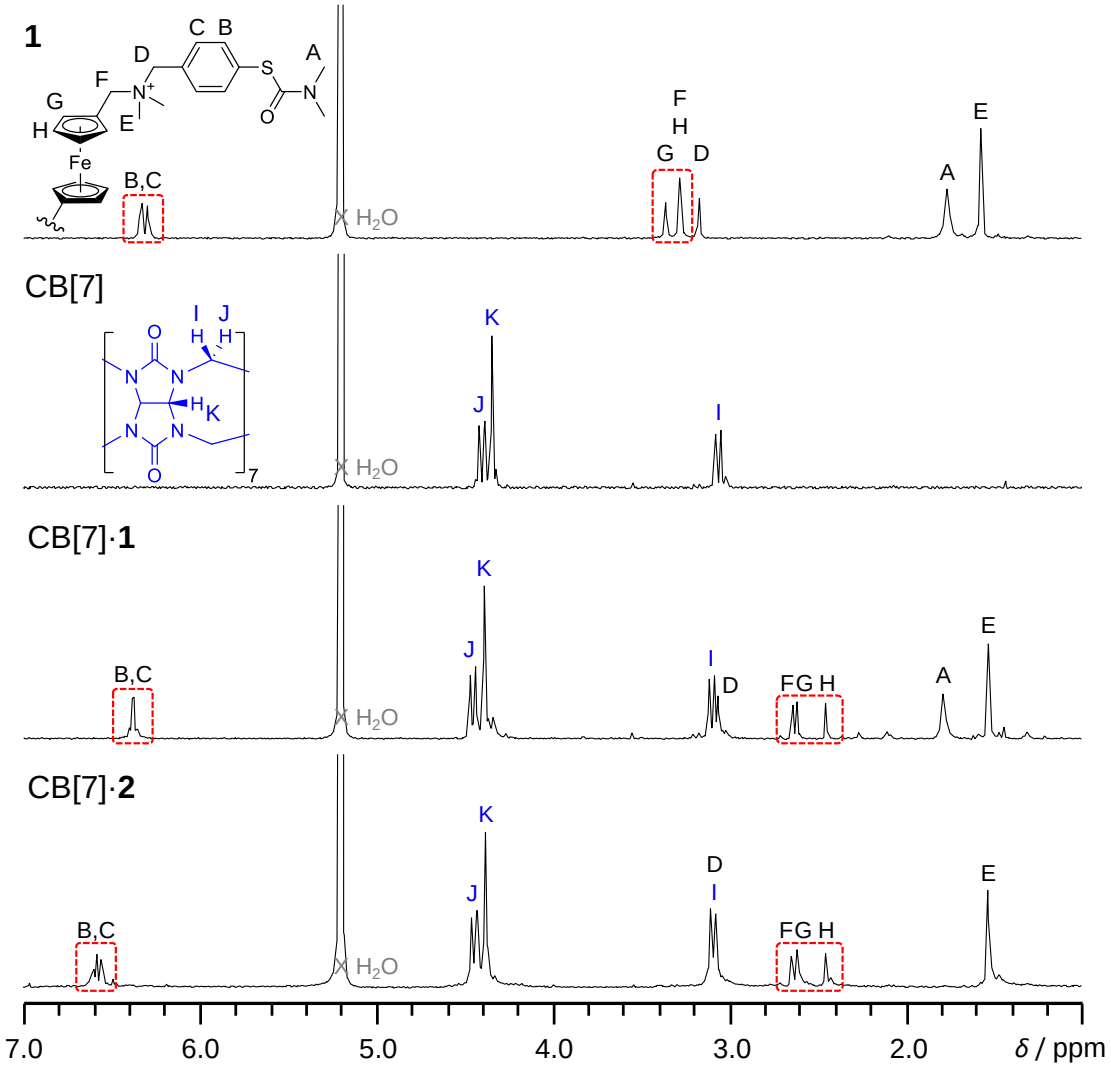

Figure S1 Stacked ^{1}H NMR spectra (100 mM KCl in 4 M $DCl_{(aq)}$, 500 MHz, 25 °C) of **1**, CB[7], CB[7]·**1**, and CB[7]·**2**. Assignment of the signals is based on the labelling shown on the structures in the figure.

S2.2. ^{1}H-^{1}H ROESY NMR spectroscopy

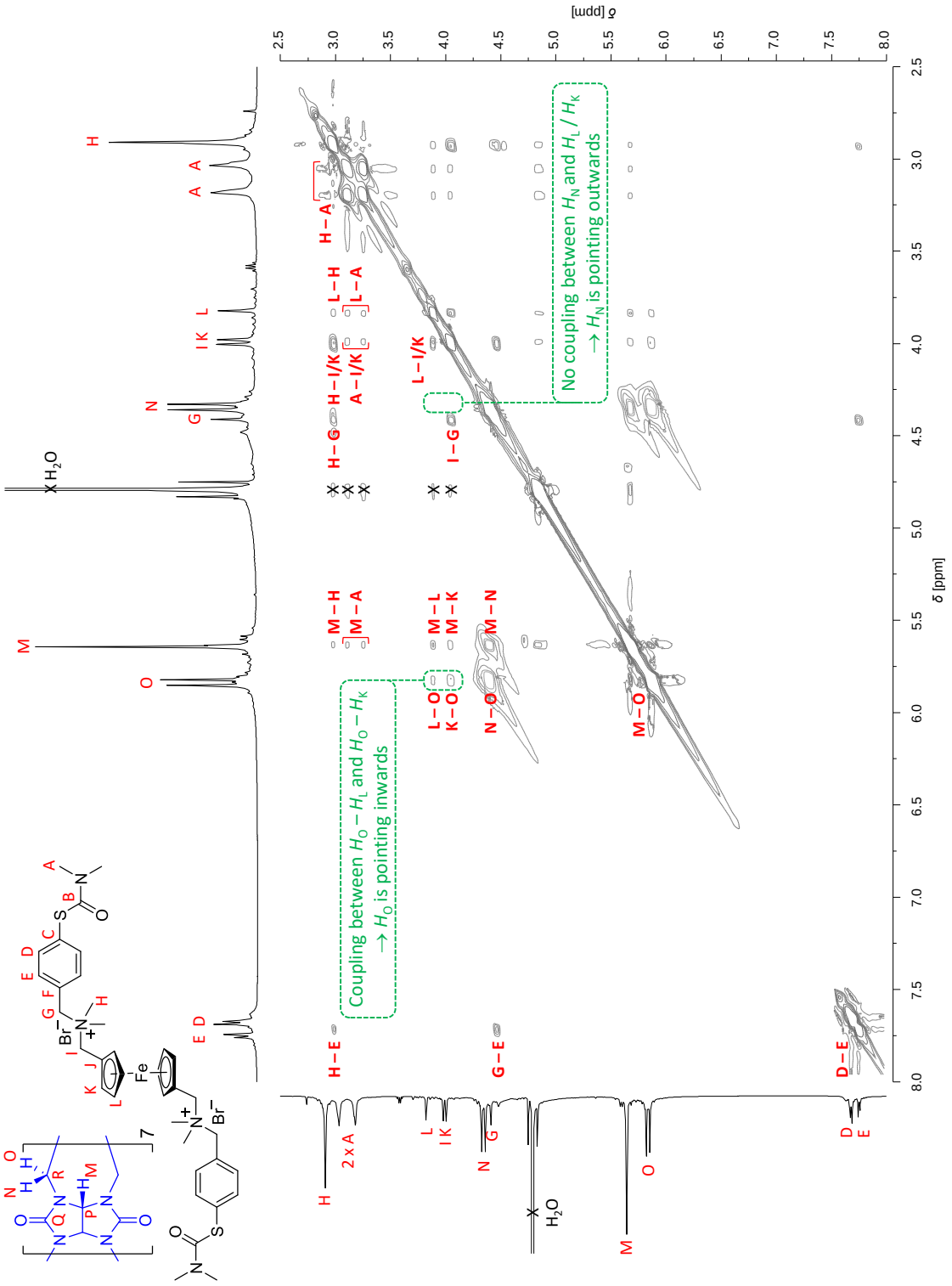

Figure S2 ^{1}H-^{1}H ROESY spectrum (100 mM KCl in D_2O, 500 MHz, 25 °C, mixing time is 0.1 sec.) of CB[7]·**1**. Assignment of the signals is based on the labelling shown on the structure in the figure.

S2.3. ^{1}H DOSY NMR spectroscopy

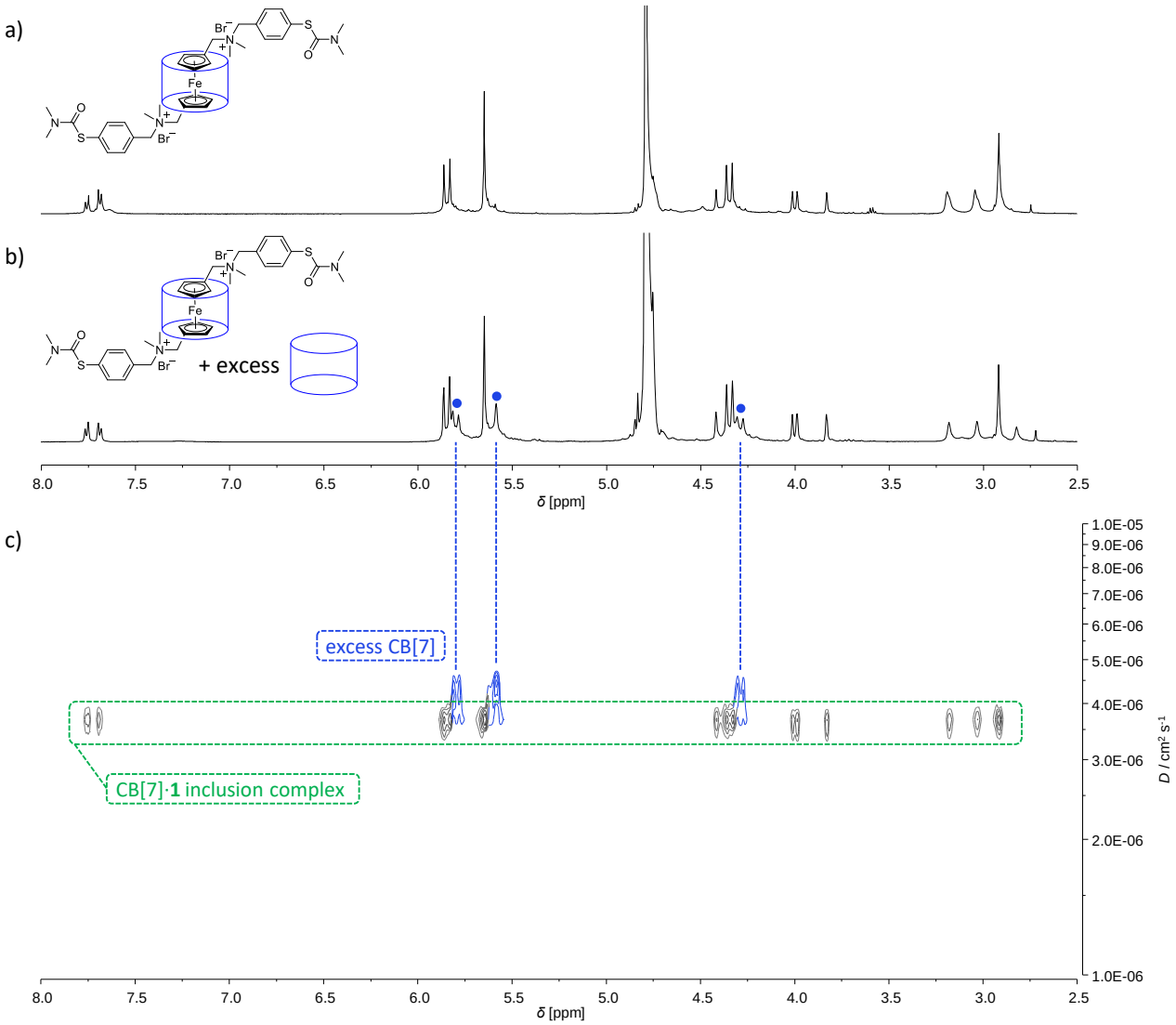

Figure S3 Stacked NMR spectra (500 MHz, 100 mM KCl in D_2O, 25 °C) showing *a*) ^{1}H NMR spectrum of CB[7]·**1**; *b*) ^{1}H NMR spectrum of CB[7]·**1** added excess CB[7], where the blue circles shows signals from excess CB[7]; and *c*) ^{1}H DOSY spectrum of CB[7]·**1** added excess CB[7], where the green circle shows signals corresponding to CB[7]·**1** ($D_{CB[7]\cdot\mathbf{1}} = 3.8 \cdot 10^{-6}$ cm^2 s^{-1}) and the blue signals arises from excess CB[7] ($D_{CB[7]} = 4.2 \cdot 10^{-6}$ cm^2 s^{-1}).

S3. Association constant determination

To determine the association constant of CB[7]·**1** a competition ^{1}H NMR spectroscopic experiment was carried out with 1,1'-bis(*N*,*N*,*N*-trimethylammoniomethyl)ferrocene (**3**) as the competitor, whose association constant to CB[7] has already been measured to be $1.9 \cdot 10^{13}$ M^{-1} in D_2O buffered with NaO_2CCD_3 (50 mM).[2]

In Figure S4 is shown the ^{1}H NMR spectra of guest **3**, CB[7]·**3**, guest **1**, CB[7]·**1**, and a mixture consisting of equimolar amounts of **1**, **3**, and CB[7]. In the latter spectrum signals of both CB[7]·**1** and CB[7]·**3** are observable meaning that both complexes coexist. Blue circles shows signals from CB[7], red circles correspond to compound **1** while green circles displays signals from **3**. The black dotted box marks the signals corresponding to the protons positioned on the ferrocene unit as well as the protons placed on the methylene bridge closet to the ferrocene unit encapsulated into CB[7]. Measurements on two more similar samples containing equimolar amounts of **1**, **3**, and CB[7] were performed and a zoom of the area of the spectra showing the before mentioned signals are shown in Figure S5.

The integration of the five signals A – E, shown in Figure S5, is given in the table below:

	Integral of signal					Total
	A	B	C	D	E	integral
Sample no. 1	0.228	0.223	0.140	0.204	0.205	1.000
Sample no. 2	0.227	0.229	0.136	0.206	0.202	1.000
Sample no. 3	0.219	0.222	0.143	0.206	0.211	1.000

Based on the integration of the signals for each complex, a ratio between the two complexes CB[7]·**1** and CB[7]·**3** can be determined. Below is shown an example with sample no. 1 where a ratio of 37:63 is found between CB[7]·**1** and CB[7]·**3**, showing how the complex CB[7]·**3** is favoured.

$$\%(\mathrm{CB[7]\cdot\mathbf{1}})_{\mathrm{No.1}} = \frac{\int \mathrm{CB[7]\cdot\mathbf{1}}}{\int(\mathrm{CB[7]\cdot\mathbf{1}} + \mathrm{CB[7]\cdot\mathbf{3}})} \cdot 100\% = \frac{0.368}{0.368 + 0.632} \cdot 100\% = 37\ \%$$

$$\%(\mathrm{CB[7]\cdot\mathbf{3}})_{\mathrm{No.1}} = \frac{\int \mathrm{CB[7]\cdot\mathbf{3}}}{\int(\mathrm{CB[7]\cdot\mathbf{1}} + \mathrm{CB[7]\cdot\mathbf{3}})} \cdot 100\% = \frac{0.632}{0.368 + 0.632} \cdot 100\% = 63\ \%$$

Similar calculations were performed for sample no. 2 and 3;

$$\frac{\%(\mathrm{CB[7]\cdot\mathbf{1}})_{\mathrm{No.2}}}{\%(\mathrm{CB[7]\cdot\mathbf{3}})_{\mathrm{No.2}}} = \frac{36\ \%}{64\ \%} \qquad \frac{\%(\mathrm{CB[7]\cdot\mathbf{1}})_{\mathrm{No.3}}}{\%(\mathrm{CB[7]\cdot\mathbf{3}})_{\mathrm{No.3}}} = \frac{36\ \%}{64\ \%}$$

Based on the assumption that the integration of the chosen proton signals is synonymous with the probability that the complex is present in the mixture at the given ratio, the association constant (K_a) for complex CB[7]·**1** in D_2O can be determined from the knowledge that K_a(CB[7]·**3**) = $1.9 \cdot 10^{13}$ M^{-1};

$$\frac{K_a(\mathrm{CB[7]\cdot\mathbf{1}})}{K_a(\mathrm{CB[7]\cdot\mathbf{3}})} = \frac{\%(\mathrm{CB[7]\cdot\mathbf{1}})}{\%(\mathrm{CB[7]\cdot\mathbf{3}})}$$

$$K_a(\mathrm{CB[7]\cdot\mathbf{1}})_{\mathrm{No.1}} = \frac{\%(\mathrm{CB[7]\cdot\mathbf{1}}) \cdot K_a(\mathrm{CB[7]\cdot\mathbf{3}})}{\%(\mathrm{CB[7]\cdot\mathbf{3}})} = \frac{37\% \cdot 1.9 \cdot 10^{13}\mathrm{M}^{-1}}{63\%} = 1.11 \cdot 10^{13}\mathrm{M}^{-1}$$

$$K_a(\mathrm{CB[7]\cdot \mathbf{1}})_{\mathrm{No.2}} = 1.08 \cdot 10^{13}\mathrm{M}^{-1} \qquad K_a(\mathrm{CB[7]\cdot \mathbf{1}})_{\mathrm{No.3}} = 1.08 \cdot 10^{13}\mathrm{M}^{-1}$$

$$K_a(\mathrm{CB[7]\cdot \mathbf{1}})_{\mathrm{Average}} = \underline{1.09 \cdot 10^{13}\mathrm{M}^{-1}}$$

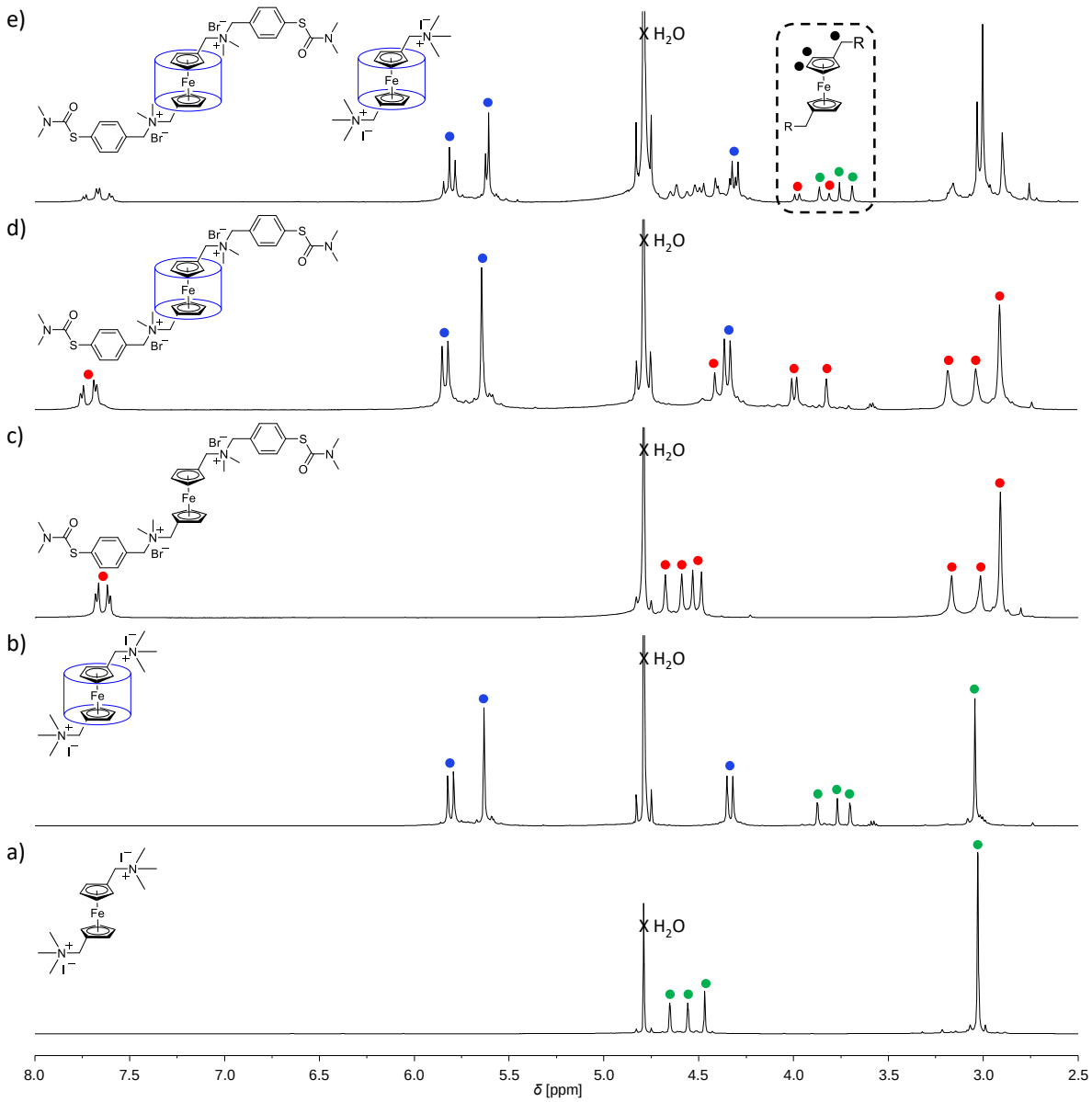

Figure S4 Stacked ^{1}H NMR spectra (500 MHz, 100 mM KCl in D_2O, 25 °C) of *a*) guest **3**; *b*) CB[7]·**3**; *c*) guest **1**; *d*) CB[7]·**1**; and *e*) a mixture consisting of equimolar amounts of **1**, **3**, and CB[7]. Blue circles shows signals from CB[7], red circles correspond to compound **1** while green circles shows **3**.

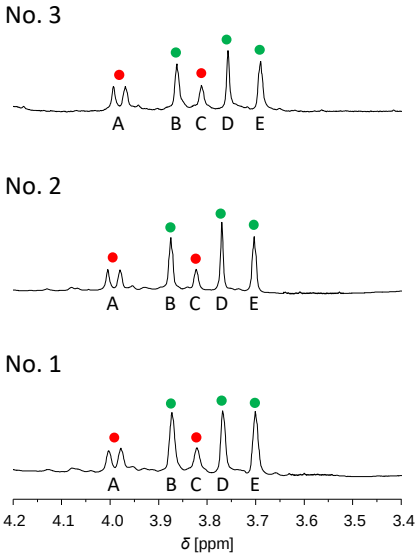

Figure S5 Zoom of ^{1}H NMR spectra (500 MHz, 100 mM KCl in D_2O, 25 °C) of three similar samples containing a mixture of equimolar amounts of **1**, **3**, and CB[7]. Red circles correspond to complex CB[7]·**1** while green circles shows CB[7]·**3**.

S4. LC/MS characterisation

Separation of **1**, CB[7]·**1**, and CB[7]·**2** were achieved using a Dionex Acclaim RSLC PolarAdvantage II (PA2) C18 2.2 µm 120 Å 2.1 × 50 mm column together with the following parameters: temperature 20 °C; flow rate 0.6 mL min^{-1}; injection volume 5 µL; wavelength 255 nm. The mobile phase solutions were 0.1 % formic acid in H_2O (A) and 0.1 % formic acid in MeCN (B). Analysis was achieved using the solvent profile outlined below;

Time [min]	% solution A	% solution B
0.0	90	10
3.5	50	50
3.6	90	10

S5. Cyclic voltammetry (CV)

S5.1. General methods

Chemicals and reagents.
KH_2PO_4 (99.995 %, Sigma-Aldrich), $HClO_4$ (99.999 %, Sigma-Aldrich), KBr (99.5 %, BDH Chemicals), and KCl (99.5 %, Merck) were used as received. Millipore water (18.2 MΩ cm) was used throughout all experiments, both for cleaning glass ware and to make the solutions used for the electrochemical measurements.

Electrochemistry measurements.
All glassware was cleaned prior to any measurements by boiling in 15% HNO_3 solution, rinsed thoroughly with Millipore water, and ultrasonicated in a Millipore water bath (2 × 30 minutes).

Cyclic voltammetry were performed using a three compartments homemade cell with a volume of 15 mL, containing a freshly prepared solution of either KH_2PO_4 (20 mM, pH 4.6) or $HClO_4$ (20 mM, pH 1.4) as electrolyte solution. A freshly prepared reversible hydrogen electrode (RHE) served as reference electrode (RE), a bright Pt wire as counter electrode (CE), and a glassy carbon (GC) electrode (4.0 mm in diameter) as working electrode (WE). The electrolyte solution was purged with purified argon for 1 hour before the electrochemical measurement was done and hereafter kept under an argon atmosphere throughout the experiment.

The surface of the GC electrode was freshly polished before each experiment with 2400 and 4000 silicon carbide papers, followed by alumina slurry (1.0, 0.3, and 0.05 µm Al_2O_3) in sequence. The electrode was cleaned thoroughly with Millipore water between each polishing step and finally ultrasonicated in a Millipore water bath (2 × 10 minutes) to remove any residual alumina.

The solubility of **1**, CB[7]·**1**, and CB[7]·**2** in aqueous solution is low, why a 50 µM solution of each target molecule in the supporting electrolyte solution was prepared by sonication for one hour prior to use.

All voltammetric measurements were carried out at room temperature (21 ± 2 °C), using an Autolab PGSTAT12 system (Metrohm Autolab B.V., Netherlands) controlled by NOVA v. 1.10 software. The RHE was calibrated against a saturated calomel electrode (SCE) after each experiment. All electrochemical potentials are reported versus SCE in this work. Argon (5.0 N) was used to degas the solution for 20 minutes and an argon flow was maintained about the solution during all electrochemical measurements.

S5.2. Additional cyclic voltammograms

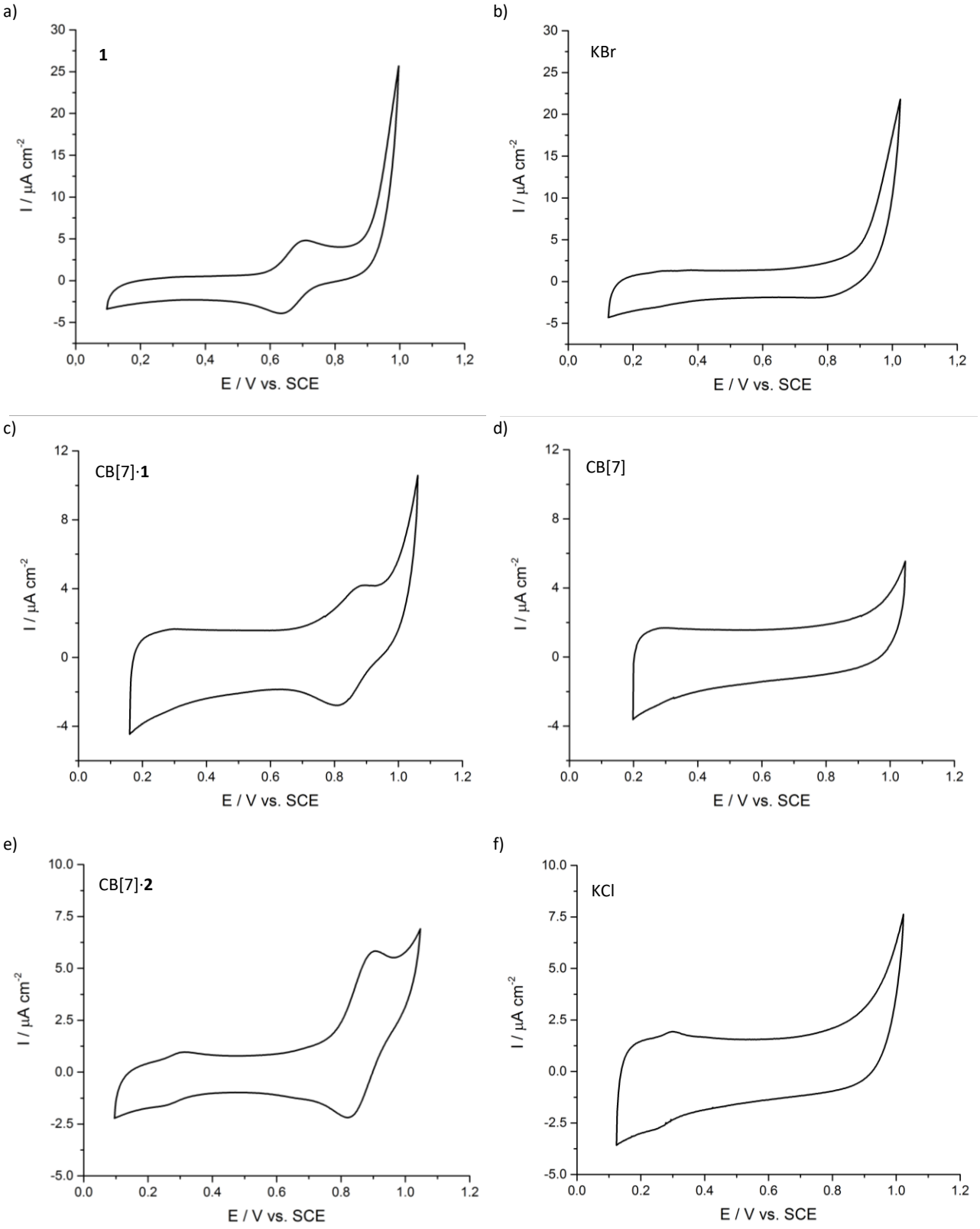

Figure S6 Cyclic voltammograms of *a*) **1** (50 µM); *b*) KBr (50 µM); *c*) CB[7]·**1** (50 µM, 1:1.3 equiv.); *d*) CB[7] (65 µM); *e*) CB[7]·**2** (50 µM); and *f*) KCl (50 µM). All compounds were measured in an aqueous 20 mM KH_2PO_4 solution (pH 4.6), scan rate 50 mV/s.

S5.3. Comparison of voltammograms

Table S1 gives an overview of the peaks observed in the cyclic voltammograms shown in Figure S6 together with the calculated midpoint redox potential ($E°$) of the examined compounds.

Table S1 Overview of the observed anodic (E_{pa}) and cathodic (E_{pc}) peaks together with the calculated midpoint redox potential ($E°$) of the examined compounds measured by cyclic voltammetry as shown in Figure S6. All potentials vs SCE.

Compound	E_{pa} [V]	E_{pc} [V]	$E°$ [V]
1	0.709	0.630	0.670
CB[7]·**1**	0.881	0.802	0.842
CB[7]·**2**	0.892	0.817	0.855
	0.308	0.247	0.278
CB[7]	–	–	–
KBr	–	–	–
KCl	0.299	0.250	0.275

By use of the Nernst equation the midpoint redox potential change (ΔE^0) can be related to a change in Gibbs free energy ($\Delta\Delta G°$) as shown in Eq. S1;

$$\Delta\Delta G^\circ = -v \cdot F \cdot \Delta E° = -1 \cdot 9.6485 \cdot 10^4 \text{ C mol}^{-1} \cdot 0.172 \text{ V} = -16.6 \text{ kJ mol}^{-1} \qquad \text{Eq. S1}$$

where v is the number of electrons transferred in the reaction and F is the Faraday constant. Table S2 gives an overview of the determined midpoint redox potential shifts of the one-electron transfer of the ferrocene moiety together with the related change in Gibbs free energy going from **1** to CB[7]·**1** and CB[7]·**2**.

Table S2 Overview of the midpoint redox potential shifts ($\Delta E°$) of the one-electron transfer of the ferrocene moiety together with the related changes in Gibbs free energy ($\Delta\Delta G°$) going from **1** to CB[7]·**1** and CB[7]·**2**.

	1	CB[7]·**1**	CB[7]·**2**
1		+ 172 mV – 16.6 kJ mol^{-1}	+ 185 mV – 17.8 kJ mol^{-1}
CB[7]·**1**			+ 13 mV – 1.25 kJ mol^{-1}
CB[7]·**2**			

S5.4. Determination of diffusion coefficients

The effect of the higher scan rate on the electrochemical response of the ferrocene peak was examined for **1**, CB[7]·**1**, and CB[7]·**2** (latter both at pH 4.6 and 1.4). The resulting voltammograms are shown in Figure S7 and the derived electrochemical parameters are collected on page 28.

a)

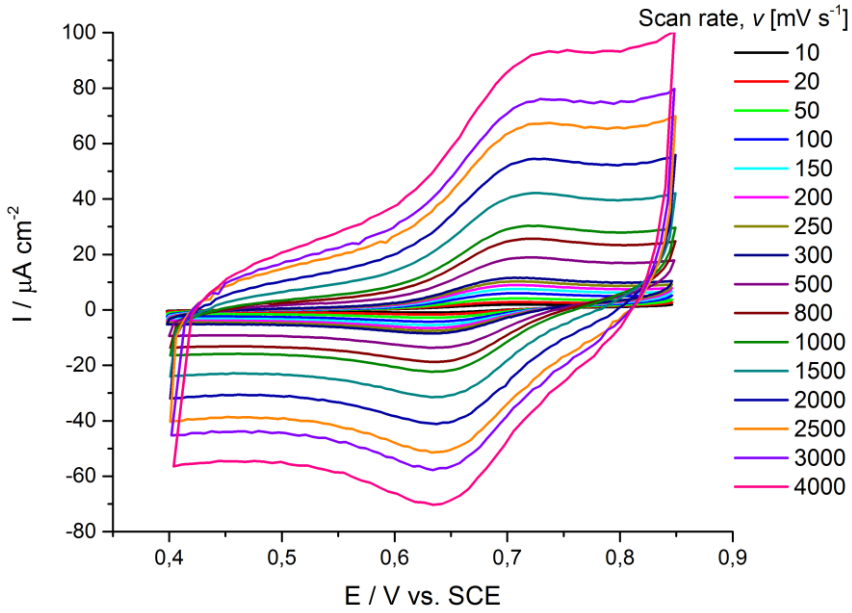

b)

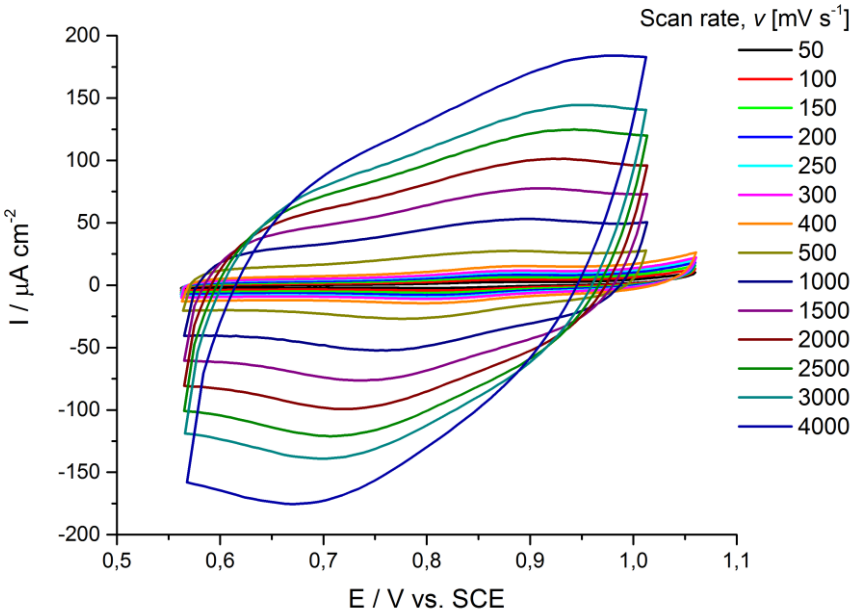

c)

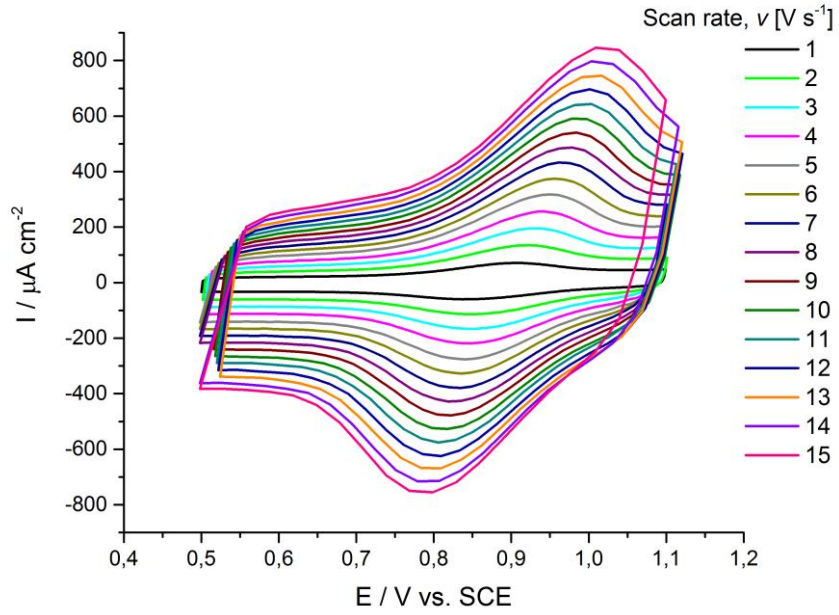

d)

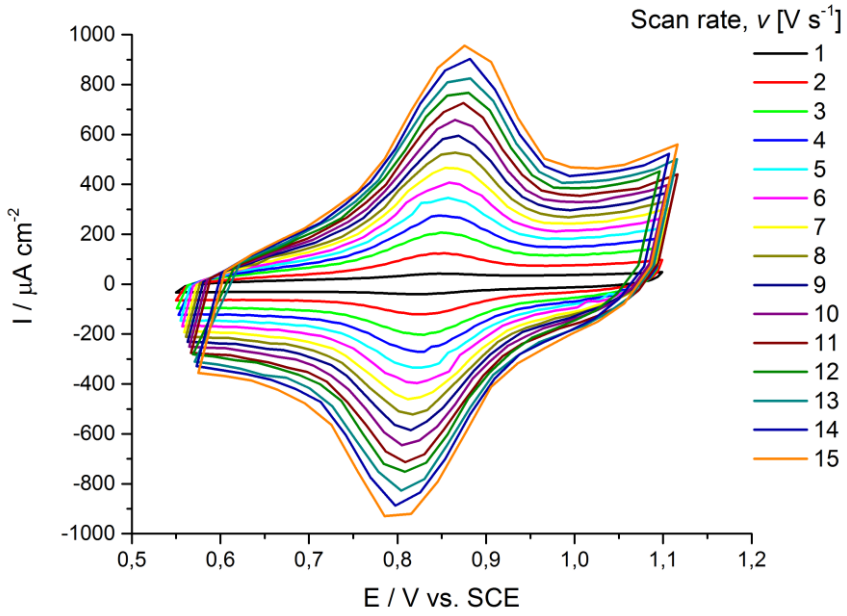

Figure S7 Cyclic voltammograms at different scan rates of *a*) **1** (50 µM, pH 4.6); *b*) CB[7]·**1** (50 µM, 1:1.3 equiv., pH 4.6); *c*) CB[7]·**2** (50 µM, pH 4.6); and *d*) CB[7]·**2** (50 µM, pH 1.4).

Figure S8 display the anodic and cathodic peak current (i_{pa} and i_{pc}) as a function of the scan rate (v) for the measurements while in Figure S9 the anodic and cathodic peak current is plotted as a function of the square root of the scan rate.

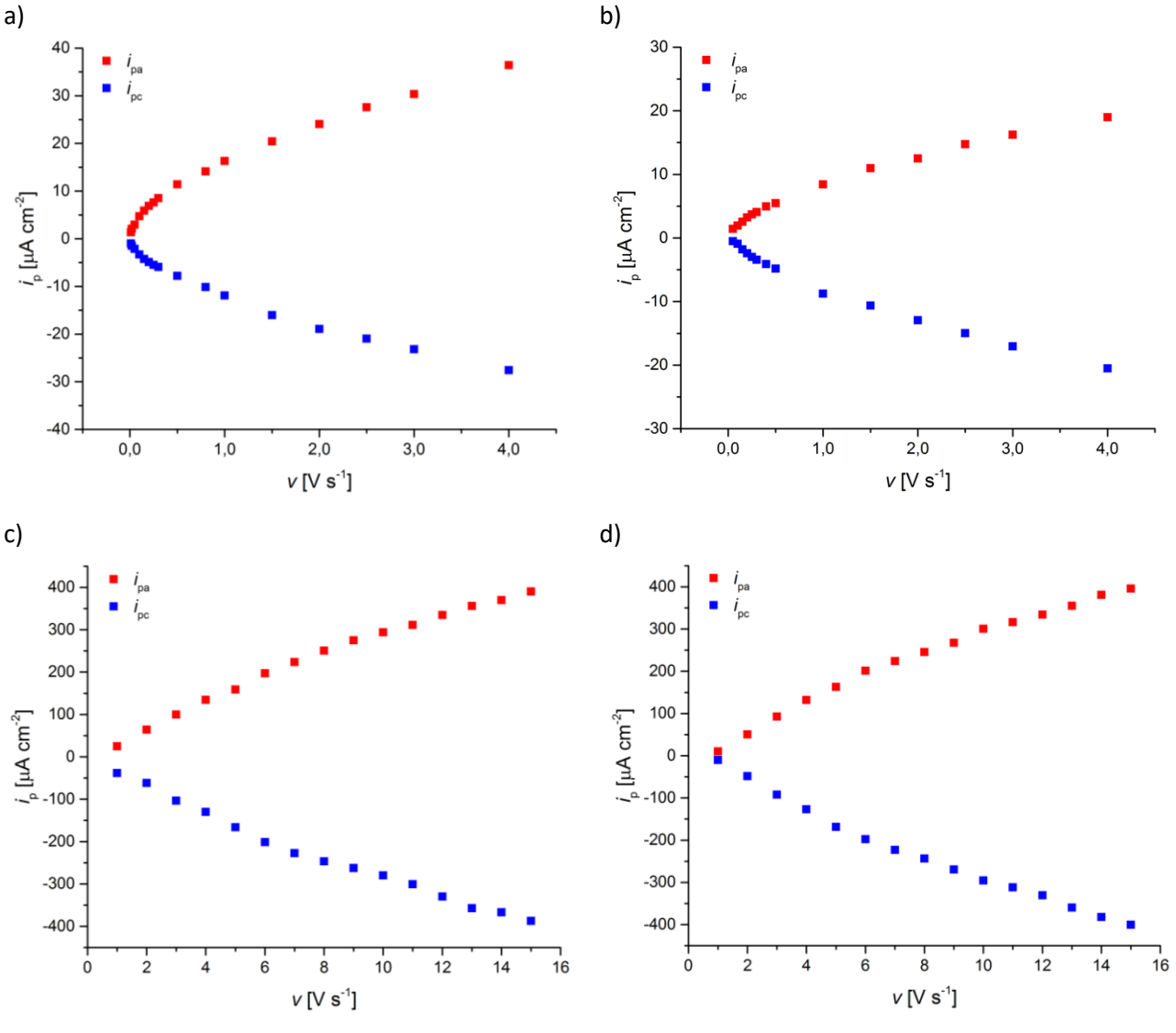

Figure S8 Plots of the peak current (i_p) as a function of the scan rate (v) for *a*) **1**; *b*) CB[7]·**1**; *c*) CB[7]·**2** (pH 4.6); and *d*) CB[7]·**2** (pH 1.4). Red squares denote the anodic peak current (i_{pa}) while blue squares represents the cathodic peak current (i_{pc}).

Figure S8 shows clearly that the electrochemical processes for **1** and CB[7]·**1** are not surfaced controlled. The surface behaviour of CB[7]·**2** is less obvious from this plot, but will be clarified in Section S5.6 below.

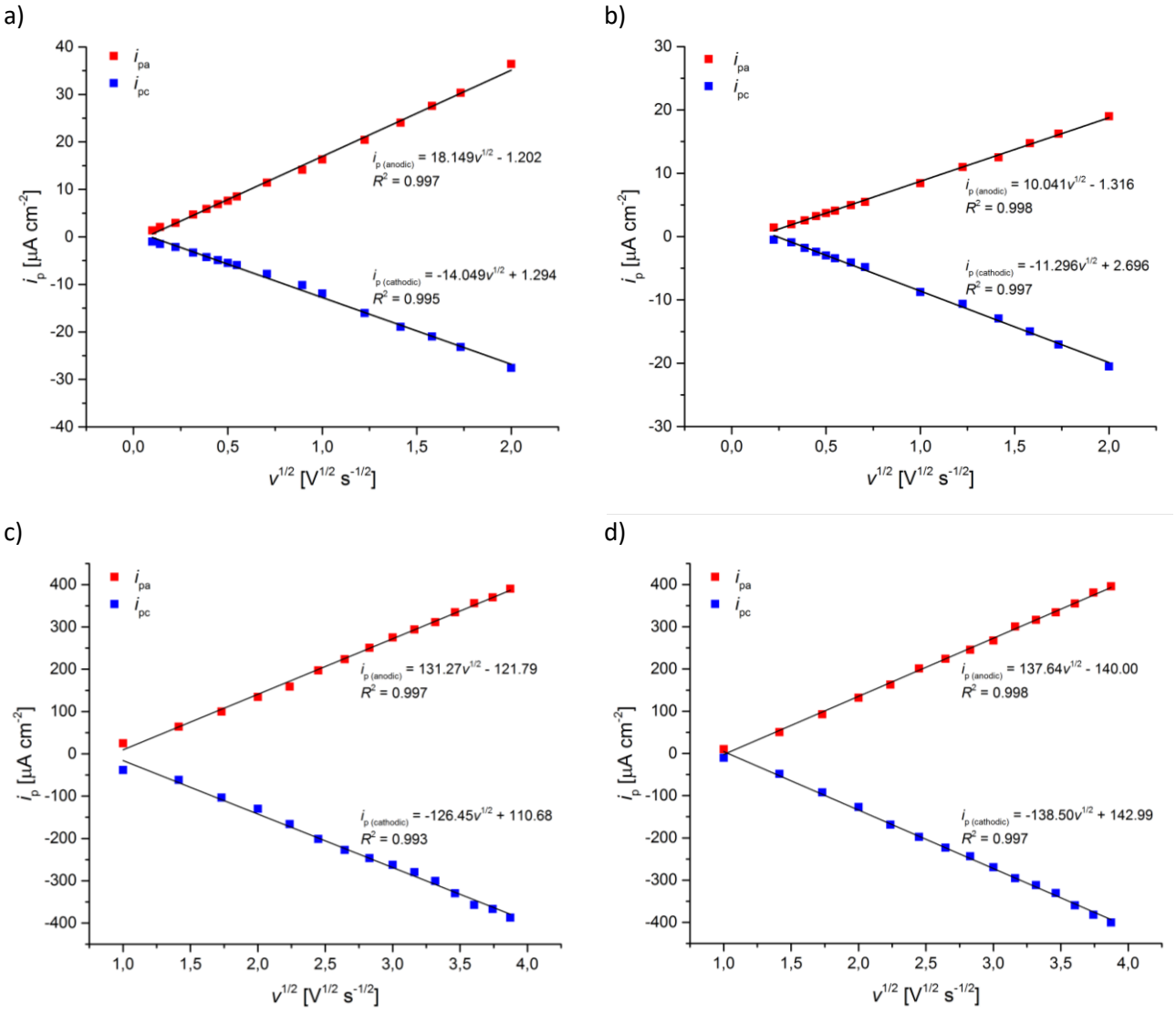

Figure S9 Plots of the peak current (i_p) as a function of the square root of the scan rate ($v^{1/2}$) for *a*) **1**; *b*) CB[7]·**1**; *c*) CB[7]·**2** (pH 4.6); and *d*) CB[7]·**2** (pH 1.4). Red squares denote the anodic peak current (i_{pa}) while blue squares represents the cathodic peak current (i_{pc}).

Figure S9 shows that electrochemical processes for **1** and CB[7]·**1** are diffusion controlled. The correlation for CB[7]·**2** is less clear and will be re-addressed in Section S5.6 below.

Quantitative information regarding the analytes diffusion coefficient can be obtained from the voltammograms in Figure S7 using the Randles-Sevcik equation (Eq. S2).[3] This equation relates the peak current (i_p, A) to the scan rate (v, V s^{-1}),

$$i_p = 0.4463 \cdot n \cdot F \cdot A \cdot c \cdot \sqrt{\frac{n \cdot F \cdot v \cdot D_0}{R \cdot T}} \qquad \text{Eq. S2}$$

In this equation, n is the number of electrons in the redox process, 1 for all target compounds 1; CB[7]·1 and CB[7]·2. F is the Faraday constant (96485 C mol^{-1}), A is the electrode area (cm^2), c is the concentration of the compound (mol cm^3), D_0 is the diffusion coefficient (cm^2 s), R is the universal gas constant (8.314 C V mol^{l-1} K^{-1}), and T is the absolute temperature (K).

By rearranging Eq. S2 into Eq. S3, it transpire how the peak current is directly proportional to the square root of the scan rate,

$$i_p = 0.4463 \cdot n^{3/2} \cdot F^{3/2} \cdot A \cdot c \cdot \sqrt{\frac{D_0}{R \cdot T}} \cdot \sqrt{v} \qquad \text{Eq. S3}$$

If the concentration of the analyte is known, the diffusion coefficient can be calculated from the slope of the linear fit of the plot i_p versus the square root of the scan rate (Eq. S4). Eq. S5 shows D_0 in its isolated form.

$$slope = 0.4463 \cdot n^{3/2} \cdot F^{3/2} \cdot A \cdot c \cdot \sqrt{\frac{D_0}{R \cdot T}} \qquad \text{Eq. S4}$$

$$D_0 = \left(\frac{slope}{0.4463 \cdot n^{3/2} \cdot F^{3/2} \cdot A \cdot c}\right)^2 \cdot R \cdot T \qquad \text{Eq. S5}$$

However, the voltammograms in Figure S7 shows the current per square centimetres (A cm^{-2}) on the y-axis thereby taking into account the area of the electrode. Therefore, the Randles-Sevcik equation (Eq. S3) can be rewritten into Eq. S6 and the diffusion coefficient is calculated as given in Eq. S7,

$$\frac{i_p}{A} = 0.4463 \cdot n^{3/2} \cdot F^{3/2} \cdot c \cdot \sqrt{\frac{D_0}{R \cdot T}} \cdot \sqrt{v} \qquad \text{Eq. S6}$$

$$D_0 = \left(\frac{slope}{0.4463 \cdot n^{3/2} \cdot F^{3/2} \cdot c}\right)^2 \cdot R \cdot T \qquad \text{Eq. S7}$$

When plotting the anodic peak current in **1** as a function of the square root of the scan rate (Figure S9a, red squares), a linear regression was found following Eq. S8,

$$i_{pa} = 18.149 \cdot 10^{-6} \cdot \sqrt{v} - 1.202 \qquad (R^2 = 0.997) \qquad \text{Eq. S8}$$

By introducing the slope from Eq. S8 into Eq. S7, the diffusion coefficient can then be determined for **1**,

$$D_0 = \left(\frac{18.149 \cdot 10^{-6} \frac{A \cdot cm^{-2}}{V^{1/2} \cdot s^{-1/2}}}{0.4463 \cdot 1^{3/2} \cdot \left(96485 \frac{C}{mol}\right)^{3/2} \cdot 50 \cdot 10^{-9} \frac{mol}{cm^3}} \right)^2 \cdot 8.314 \frac{C \cdot V}{mol \cdot K} \cdot 298K \qquad \text{Eq. S9}$$

$$D_0 = 1.825 \cdot 10^{-6}\, cm^2/s$$

In the same way, the diffusion coefficient can be determined for **1** based on the cathodic peak current as well as the corresponding values for CB[7]·**1** and CB[7]·**2** These are collected in Table S3.

Table S3 Overview of the functions obtained when plotting the anodic and cathodic peak current as a function of the square root of the scan rate (Figure S9) of the voltammograms given in Figure S7 of **1**, CB[7]·**1**, and CB[7]·**2**, their R^2 values, and the corresponding derived diffusion coefficients (D_0).

Compound	pH	i_p versus $\sqrt{v}$	R^2	D_0 [cm^2 s^{-1}]	$D_{0\,(average)}$ [cm^2 s^{-1}]
1	4.6	$i_{pa} = 18.2 \cdot 10^{-6} \cdot \sqrt{v} - 1.20$	0.997	$1.8 \cdot 10^{-6}$	$(1.5 \pm 0.4) \cdot 10^{-6}$
		$i_{pc} = -14.0 \cdot 10^{-6} \cdot \sqrt{v} + 1.29$	0.995	$1.1 \cdot 10^{-6}$	
CB[7]·**1**	4.6	$i_{pa} = 10.0 \cdot 10^{-6} \cdot \sqrt{v} - 1.32$	0.998	$5.6 \cdot 10^{-7}$	$(6.3 \pm 0.7) \cdot 10^{-7}$
		$i_{pc} = -11.3 \cdot 10^{-6} \cdot \sqrt{v} + 2.70$	0.997	$7.1 \cdot 10^{-7}$	
CB[7]·**2**	4.6	$i_{pa} = 131 \cdot 10^{-6} \cdot \sqrt{v} - 122$	0.997	$9.5 \cdot 10^{-5}$	$(9.2 \pm 0.3) \cdot 10^{-5}$
		$i_{pc} = -127 \cdot 10^{-6} \cdot \sqrt{v} + 111$	0.993	$8.9 \cdot 10^{-5}$	
	1.4	$i_{pa} = 138 \cdot 10^{-6} \cdot \sqrt{v} - 140$	0.998	$10.5 \cdot 10^{-5}$	$(10.6 \pm 0.1) \cdot 10^{-5}$
		$i_{pc} = -139 \cdot 10^{-6} \cdot \sqrt{v} + 143$	0.997	$10.6 \cdot 10^{-5}$	

S5.5. Determination of diffusion controlled electron transfer rate constants

Figure S10 shows the ratio of the oxidation peak current to its corresponding reduction counterpart ($i_{p\,(anodic)}/i_{p\,(cathodic)}$) plotted as a function of the scan rate. It is seen for all cases that the ratio of the peak currents is close to one when one disregards the uncertainty that are on the first measurements.

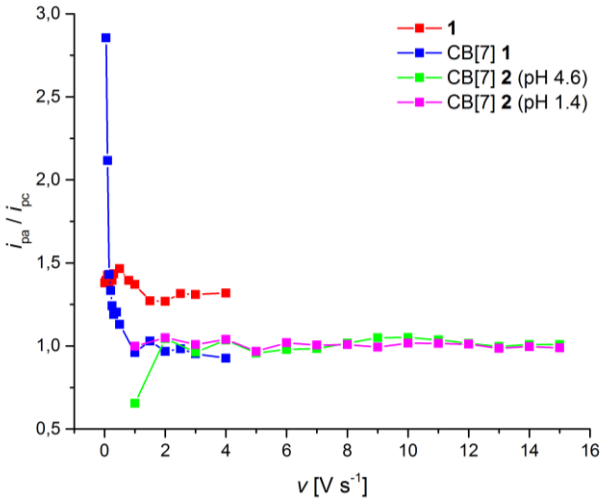

Figure S10 Plots of the peak current ratio (i_{pa} / i_{pc}) as a function of the scan rate (v) for **1** (red), CB[7]·**1** (blue), CB[7]·**2** (pH 4.6, green), and CB[7]·**2** (pH 1.4, purple).

Figure S11a shows the peak potential separation plotted as a function of the scan rate for **1**, CB[7]·**1**, and CB[7]·**2**. Here it is apparent, how the electrochemical reversibility in **1** changes from a reversible process ($0.01 < v < 0.50$) to a quasi-reversible process ($0.50 < v$) when increasing the scan rate (zoom is shown in Figure S11b). In comparison, CB[7]·**1** and CB[7]·**2** remains quasi-reversible processes at all scan rates.

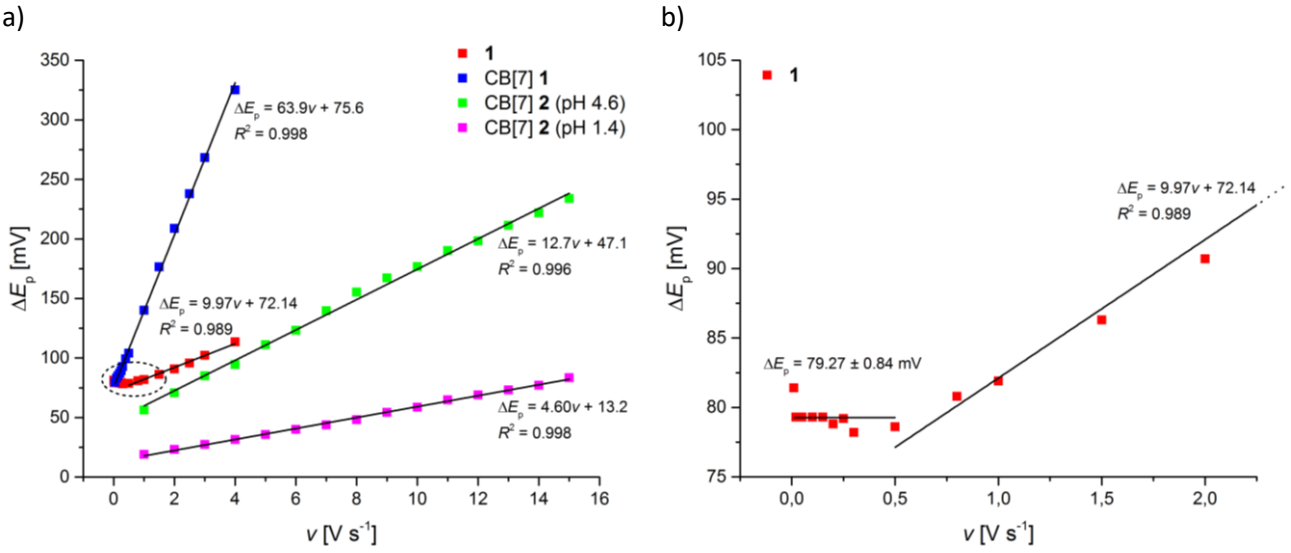

Figure S11 Plots of *a*) peak potential separation (ΔE_p) as a function of the scan rate (v) for **1** (red), CB[7]·**1** (blue), CB[7]·**2** (pH 4.6, green), and CB[7]·**2** (pH 1.4, purple) and *b*) a zoom of **1** at low scan rates.

The heterogeneous electron transfer rate constant can be determined for quasi-reversible processes using a method relating the rate constant to the difference in peak potential called the Nicholson Method (Eq. S10),[4]

$$\Psi = \frac{\gamma^{\alpha} \cdot k_s}{\sqrt{D_0 \cdot \pi \cdot a}} \qquad \text{Eq. S10}$$

Here, Ψ is a kinetic, dimensionless parameter that is tabulated as a function of the difference in peak potential, $\gamma^{\alpha} = D_o/D_R$ where D_0 and D_R are the diffusion coefficients of the oxidised and reduced species, α is the charge transfer coefficient, while $a = n \cdot F \cdot v/R \cdot T$.

The literature values of Ψ are given below in Figure S12 together with a plot showing ΔE_p as a function of Ψ.[4] The graph is used to derive the specific Ψ value at a given difference in peak potential.

a)

Ψ	ΔE_p [mV]
5.00	65
4.00	66
3.00	68
2.00	72
1.00	84
0.75	92
0.50	105
0.35	121
0.25	141
0.10	212

b)

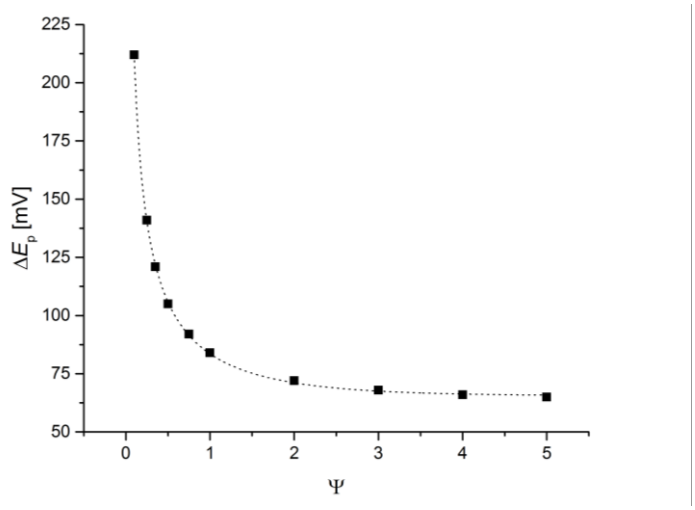

Figure S12 *a*) Literature values of Ψ to its corresponding peak potential separation (ΔE_p) and *b*) a plot showing ΔE_p as a function of Ψ.[4]

It has to be noted that Nicholson's method only applies for quasi-reversible processes, which has a peak separation in the range 57 to 200 mV since a smaller peak separation indicates a reversible process while larger peak separations shows an irreversible process.

Following standard procedure, $D_0 = D_R$ and α = 0.5, Eq. S10 can be rewritten into Eq. S11,

$$k_s = \Psi \sqrt{D_0 \cdot \pi \cdot \frac{n \cdot F \cdot v}{R \cdot T}} \qquad \text{Eq. S11}$$

The heterogeneous electron transfer rate constant for a given compound at the various applied scan rates can then be calculated using the diffusion coefficient determined previously while the value used for Ψ is determined from the graph above at a given peak separation.

Eq. S12 shows an example of the calculation of a rate constant for **1** at a scan rate of 0.5 V s^{-1} where the observed peak potential separation of 78.6 mV corresponds to a value of 1.22 for Ψ,

$$k_s = 1.22\sqrt{1.5 \cdot 10^{-6}\, cm^2/s \cdot \pi \cdot \frac{1 \cdot 96485 \frac{C}{mol} \cdot 0.5V \cdot s^{-1}}{8.314 \frac{C \cdot V}{mol \cdot K} \cdot 298K}} = 1.15 \cdot 10^{-2}\, cm/s \qquad \text{Eq. S12}$$

The rate constants at the remaining scan rates applied can be calculated similarly and then plotted as a function of the scan rate to derive the average rate constant.

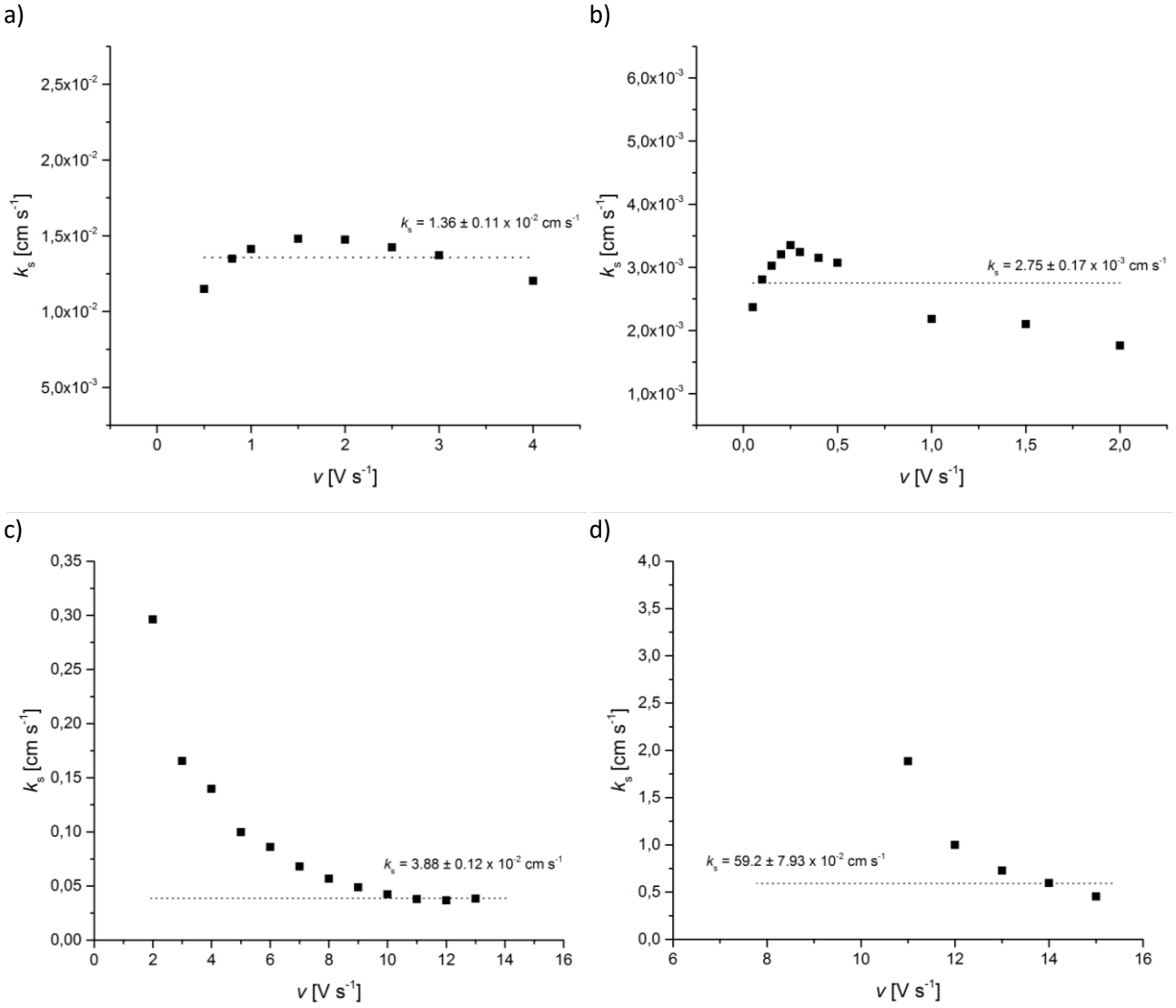

Figure S13 Plot of the heterogeneous electron transfer rate constant (k_s) as a function of the scan rate (v) for *a*) **1**; *b*) CB[7]·**1**; *c*) CB[7]·**2** (pH 4.6, calculation made on last four data points); and *d*) CB[7]·**2** (pH 1.4, calculation made on last three data points).

S5.6. Laviron analysis for CB[7]·2 at higher scan rates

Figure S14 shows the logarithmic peak current [log($i_{pa,c}$)] as a function of the logarithmic scan rate [log(v^x)], where x is a free parameter, ½ < x < 1. This a more general version of the $i_{pa,c}/v$ correlation than the limiting $i_{pa,c}/v$ and $i_{pa,c}/v^{½}$ correlations shown previously (Figure S8 and Figure S9). These new correlations illuminate further the degree of non-ideality in the limiting plots shown in Figure S8 and Figure S9.

As stated previously, the free molecule **1** accords closely with a pure diffusion controlled electron transfer process. So does, largely, CB[7]·**1,** although only for scan rates lower than about 50 mV s^{-1}. CB[7]·**2** displays, however, a value of x much closer to unity and therefore rather closer to monolayer voltammetry behaviour, although still with some non-ideality and indications of bimodal behaviour (Figure S14c and d).

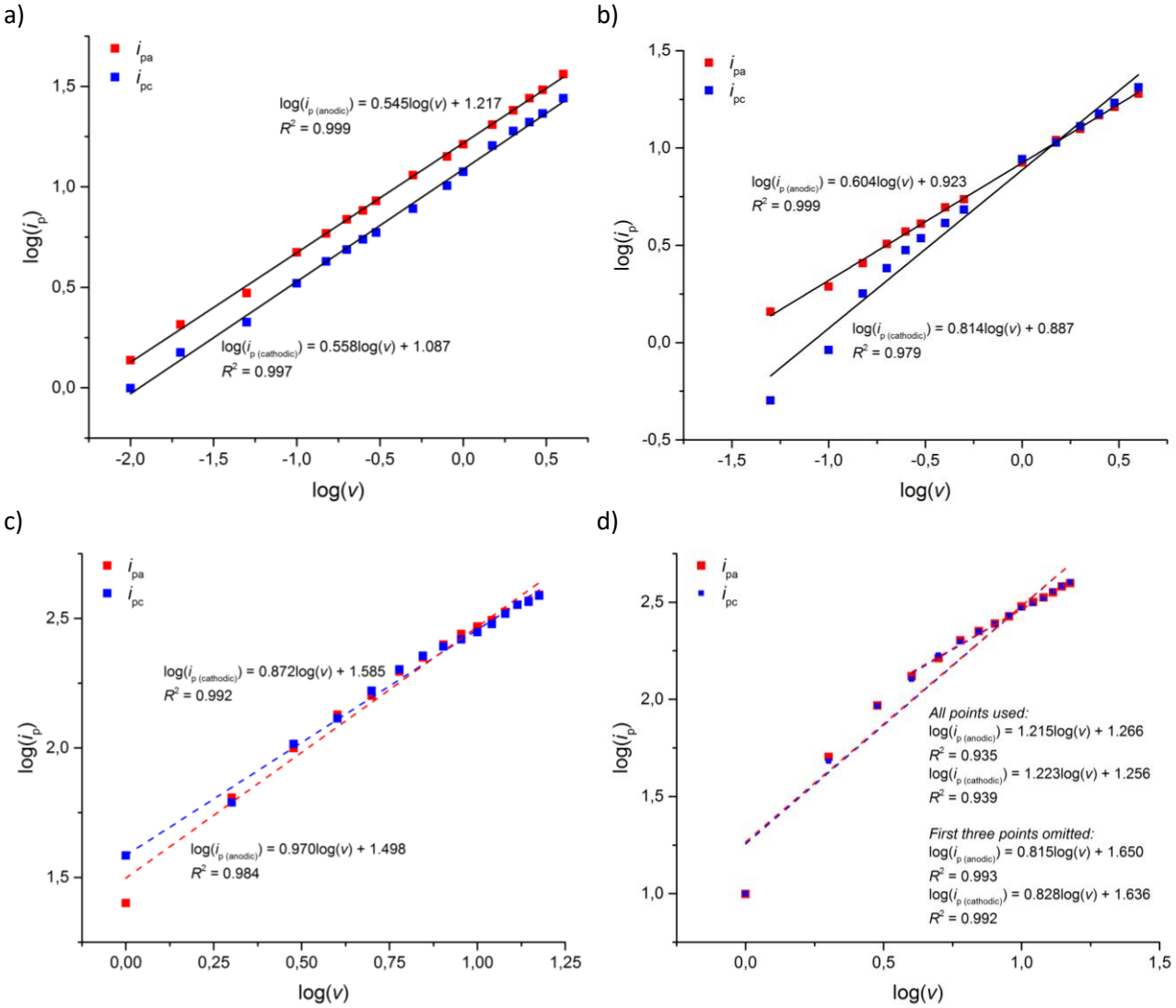

Figure S14 Plots of the logarithmic peak current [log($i_{pa,c}$)] as a function of the logarithmic scan rate [log(v^x)] for *a*) **1**; *b*) CB[7]·**1**; *c*) CB[7]·**2** (pH 4.6); and *d*) CB[7]·**2** (pH 1.4). Red squares denote the anodic peak current (i_{pa}) while blue squares represents the cathodic peak current (i_{pc}).

The interfacial electron transfer rate constant (k_s) for CB[7]·**2** was calculated using the Laviron equation (Eq. S13),[5]

$$\Delta E_p = \frac{4 \cdot R \cdot T}{n \cdot F} \cdot \ln\left(\frac{½}{m}\right) \qquad \text{Eq. S13}$$

Where the Laviron parameter, *m*, is defined as

$$m = \frac{R \cdot T \cdot k_s}{n \cdot F \cdot v} \qquad \text{Eq. S14}$$

Using these equations, k_s was found to be about 40 s^{-1} for CB[7]·**2** independent of the scan rate in the range 5-15 V s^{-1}.

S5.7. Raw data from experiments at higher scan rates

Below are collected the raw data from the experiments performed at high scan rates on **1**, CB[7]·**1**, and CB[7]·**2** (latter both at pH 4.6 and 1.4). Values of the anodic and cathodic peak currents (i_{pa} and i_{pc}), peak current ratios (i_{pa} / i_{pc}), anodic and cathodic peak potentials (E_{pa} and E_{pc}), and peak potential separations (ΔE_p) at different scan rates (v) are given.

*Compound **1** (pH 4.6)*

v [V s^{-1}]	$v^{1/2}$ [$V^{1/2}$ $s^{-1/2}$]	i_{pa} [µA cm^{-2}]	i_{pc} [µA cm^{-2}]	i_{pa} / i_{pc}	E_{pa} [mV]	E_{pc} [mV]	ΔE_p [mV]
0.01	0.10	1.37	-0.99	1.38	710.7	629.3	81.4
0.02	0.14	2.07	-1.50	1.38	709.3	630.0	79.3
0.05	0.22	2.96	-2.12	1.39	709.3	630.0	79.3
0.10	0.32	4.72	-3.31	1.43	709.3	630.0	79.3
0.15	0.39	5.87	-4.25	1.38	709.3	630.0	79.3
0.20	0.45	6.89	-4.87	1.41	709.3	630.5	78.8
0.25	0.50	7.63	-5.47	1.39	711.3	632.1	79.2
0.30	0.55	8.51	-5.93	1.43	709.3	631.1	78.2
0.50	0.71	11.41	-7.79	1.47	717.3	638.7	78.6
0.80	0.89	14.14	-10.14	1.39	722.2	641.4	80.8
1.00	1.00	16.29	-11.89	1.37	722.2	640.3	81.9
1.50	1.22	20.40	-16.04	1.27	725.6	639.3	86.3
2.00	1.41	24.05	-18.95	1.27	729.1	638.4	90.7
2.50	1.58	27.59	-20.97	1.32	731.1	635.4	95.7
3.00	1.73	30.35	-23.17	1.31	737.1	634.9	102.2
4.00	2.00	36.39	-27.60	1.32	745.4	631.9	113.5

*Complex CB[7]·**1** (pH 4.6)*

v [V s^{-1}]	$v^{1/2}$ [$V^{1/2}$ $s^{-1/2}$]	i_{pa} [µA cm^{-2}]	i_{pc} [µA cm^{-2}]	i_{pa} / i_{pc}	E_{pa} [mV]	E_{pc} [mV]	ΔE_p [mV]
0.05	0.22	1.44	-0.51	2.86	881.4	802.0	79.4
0.10	0.32	1.94	-0.92	2.12	885.3	802.0	83.3
0.15	0.39	2.56	-1.79	1.43	887.3	802.0	85.3
0.20	0.45	3.21	-2.41	1.33	889.3	802.0	87.3
0.25	0.50	3.71	-2.99	1.24	889.3	800.0	89.3
0.30	0.55	4.09	-3.43	1.19	892.0	799.3	92.7
0.40	0.63	4.95	-4.11	1.20	895.7	796.5	99.2
0.50	0.71	5.46	-4.83	1.13	893.9	789.8	104.1
1.00	1.00	8.43	-8.78	0.96	896.5	756.5	140.0
1.50	1.22	10.96	-10.65	1.03	911.3	734.8	176.5
2.00	1.41	12.52	-12.94	0.97	927.9	719.0	208.9
2.50	1.58	14.73	-14.99	0.98	943.8	705.9	237.9
3.00	1.73	16.24	-17.04	0.95	967.9	699.7	268.2
4.00	2.00	19.00	-20.51	0.93	996.1	671.1	325.0

*Complex CB[7]·**2** (pH 4.6)*

v [V s^{-1}]	$v^{1/2}$ [$V^{1/2}$ $s^{-1/2}$]	i_{pa} [µA cm^{-2}]	i_{pc} [µA cm^{-2}]	i_{pa} / i_{pc}	E_{pa} [mV]	E_{pc} [mV]	ΔE_p [mV]
1.0	1.00	25.2	-38.5	0.66	907.7	851.4	56.3
2.0	1.41	64.3	-61.6	1.04	919.8	849.1	70.7
3.0	1.73	99.9	-103.7	0.96	931.7	846.7	85.0
4.0	2.00	134.4	-129.8	1.04	938.8	844.3	94.5
5.0	2.24	159.0	-166.1	0.96	950.8	839.6	111.2
6.0	2.45	196.9	-201.2	0.98	958.0	834.8	123.2
7.0	2.65	223.5	-227.1	0.98	967.4	827.7	139.7
8.0	2.83	250.4	-246.4	1.02	975.9	820.6	155.3
9.0	3.00	275.3	-262.2	1.05	983.1	815.9	167.2
10.0	3.16	294.0	-279.9	1.05	987.8	811.1	176.7
11.0	3.32	311.5	-300.4	1.04	996.7	806.4	190.3
12.0	3.47	334.9	-329.6	1.02	1000	801.6	198.4
13.0	3.61	356.2	-357.1	1.00	1007	795.9	211.3
14.0	3.74	369.9	-366.6	1.01	1012	790.2	221.8
15.0	3.87	390.2	-387.2	1.01	1017	782.7	234.0

*Complex CB[7]·**2** (pH 1.4)*

v [V s^{-1}]	$v^{1/2}$ [$V^{1/2}$ $s^{-1/2}$]	i_{pa} [µA cm^{-2}]	i_{pc} [µA cm^{-2}]	i_{pa} / i_{pc}	E_{pa} [mV]	E_{pc} [mV]	ΔE_p [mV]
1.0	1.00	10.0	-10.0	1.00	849.5	830.4	19.1
2.0	1.41	50.6	-48.1	1.05	851.6	828.3	23.3
3.0	1.73	93.0	-92.2	1.01	853.6	826.2	27.4
4.0	2.00	131.7	-126.7	1.04	855.7	824.1	31.6
5.0	2.24	163.1	-168.6	0.97	857.8	822.1	35.7
6.0	2.45	201.4	-197.5	1.02	859.9	819.9	40.0
7.0	2.65	224.4	-223.2	1.01	861.7	817.9	43.8
8.0	2.83	245.6	-243.6	1.01	864.0	815.8	48.2
9.0	3.00	267.4	-269.3	0.99	868.2	813.8	54.4
10.0	3.16	300.3	-295.5	1.02	870.3	811.7	58.6
11.0	3.32	316.4	-311.8	1.01	874.4	809.6	64.8
12.0	3.47	334.4	-330.8	1.01	876.5	807.5	69.0
13.0	3.61	354.9	-359.8	0.99	878.6	805.5	73.1
14.0	3.74	380.9	-382.4	1.00	880.6	803.4	77.2
15.0	3.87	396.1	-400.5	0.99	882.7	799.2	83.5

S6. Connecting gold nanoparticles

S6.1 General methods

Citrate stabilized gold nanoparticles (diameter 60 nm) was purchased from Sigma-Aldrich. Citrate stabilised gold nanoparticles (diameter 12 nm) was synthesised following a previously reported method.[6] Centrifugation was carried out using an Eppendorf Mini Spin rotor KL125 (9 cm). Transmission electron microscopy was performed on a Tecnai T20 LaB6, FEI instrument.

S6.2 Self-assembly with 60 nm gold nanoparticles

In a typical experiment to prepare the gold nanoparticle dimers, citrate stabilized 60 nm gold nanoparticles (1,9E+10 particles/mL, Aldrich, product number 742015, OD = 1, absorption peak 538-544 nm) in water (1 mL) was mixed with 1 µM CB[7]·**2** solution (10 µL). In order to allow thiol-gold chemical bonding between the gold nanoparticles and CB[7]·**2** to form, the samples were allowed to mix for 6 hours. The solutions were hereafter used immediately after centrifugation (5000 rpm, 10 minutes [Centrifuge Eppendorf Mini Spin rotor KL125 (9 cm)]) to remove excess citrate. The nanoparticles were immobilized on a TEM grid (Support Films, Formvar, 200 mesh, Cu, TED PELLA, INC) precoated with poly-lysine. TEM grid was incubated with 0.25 mg/mL of poly-lysine solution for 5 minutes to increase adhesion and obtain a more uniform distribution of particles on the surface. Then the above nanoparticle solution was applied and left for several minitutes to be adsorbed on the surface. Figure S15 shows a reference experiment without the addition of CB[7]·**2** while Figure S16 shows resulting TEM micrographs with CB[7]·**2** added.

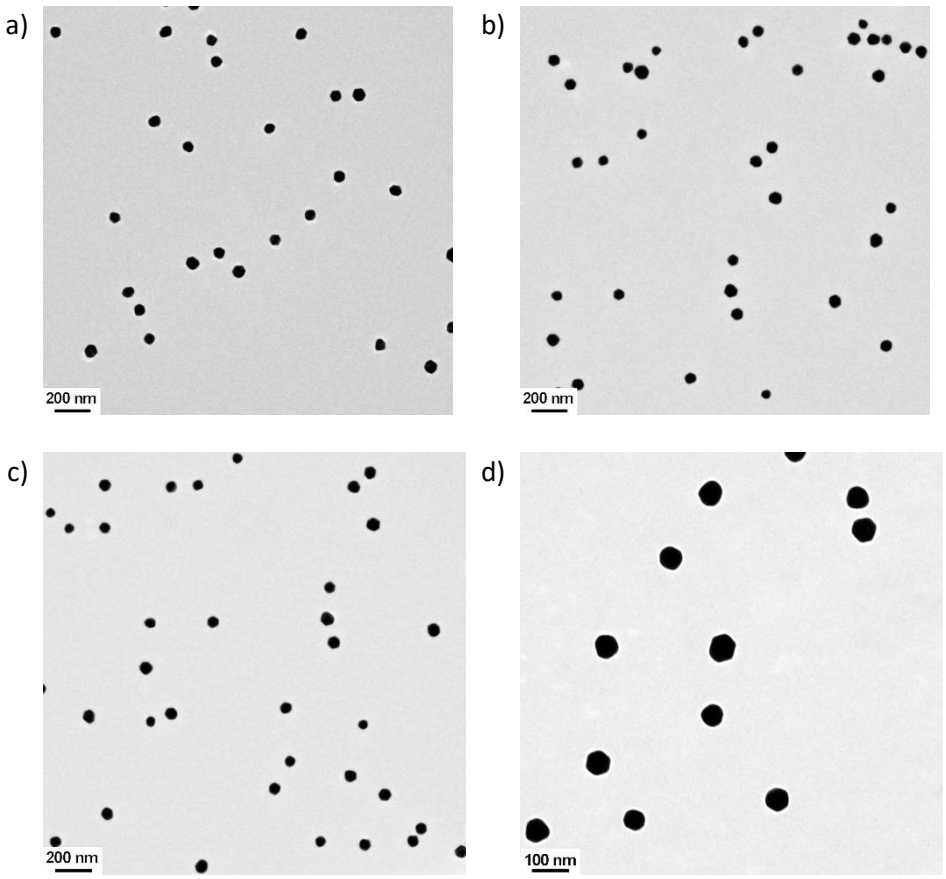

Figure S15 TEM images of the 60 nm gold nanoparticles without addition of CB[7]·**2**.

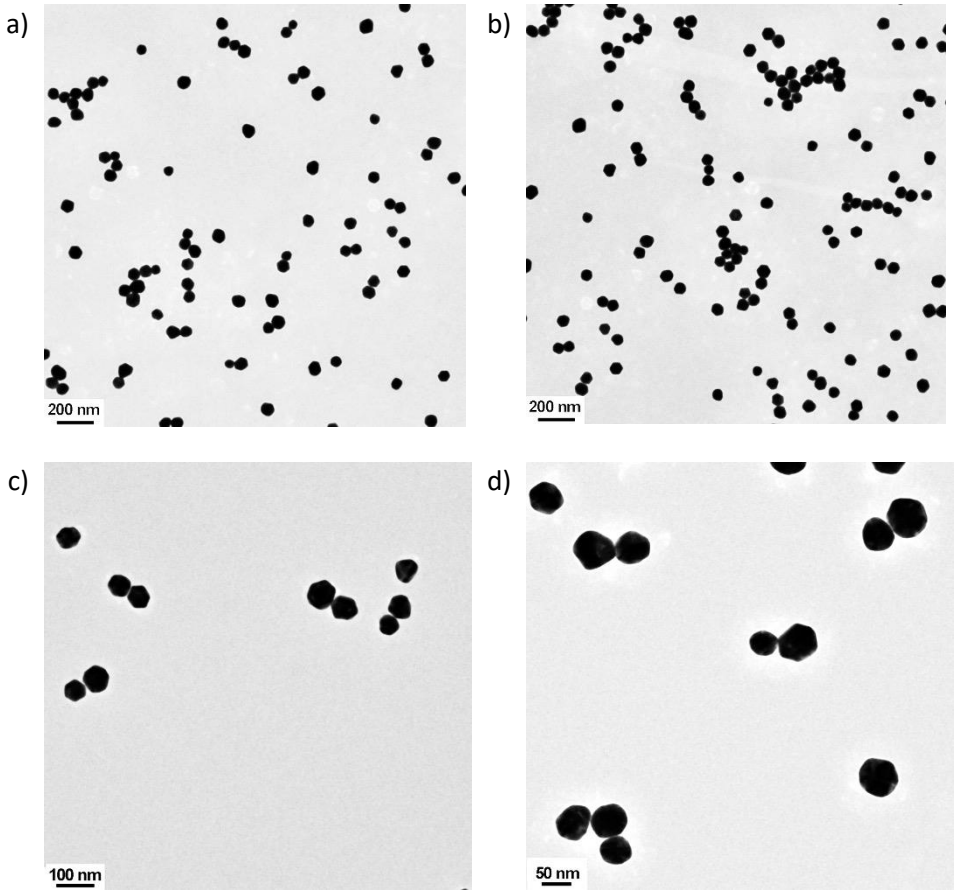

Figure S16 TEM images of the gold nanoparticle capped [2]rotaxane formed between 60 nm gold nanoparticles and CB[7]·**2**.

S6.3 Self-assembly with 12 nm gold nanoparticles

12 nm AuNP was synthesized according to a literature procedure.[7] In brief, to a rapidly-stirred boiling solution of $HAuCl_4$ (1.0 mM, 20 mL), 2 mL of a 1 % solution of trisodium citrate dehydrate ($Na_3C_6H_5O_7 \cdot 2\ H_2O$) was added quickly. The gold sol gradually forms as the citrate reduces the gold(III). The reaction mixture was removed from the heat when the solution turned deep red or 10 minutes had elapsed.

The resulting citrate stabilized 12 nm gold nanoparticles in water (1 mL) was mixed with 1 µM CB[7]·**2** solution (10 µL). In order to allow thiol-gold chemical bonding between the gold nanoparticles and CB[7]·**2** to form, the samples were allowed to react for 6 hours. The solutions were hereafter used immediately after centrifugation (5000 rpm, 10 minutes) to remove excess citrate. The TEM images (Figure S17) show that the gold nanoparticles are self-assembled by the linkage of CB[7]·2.

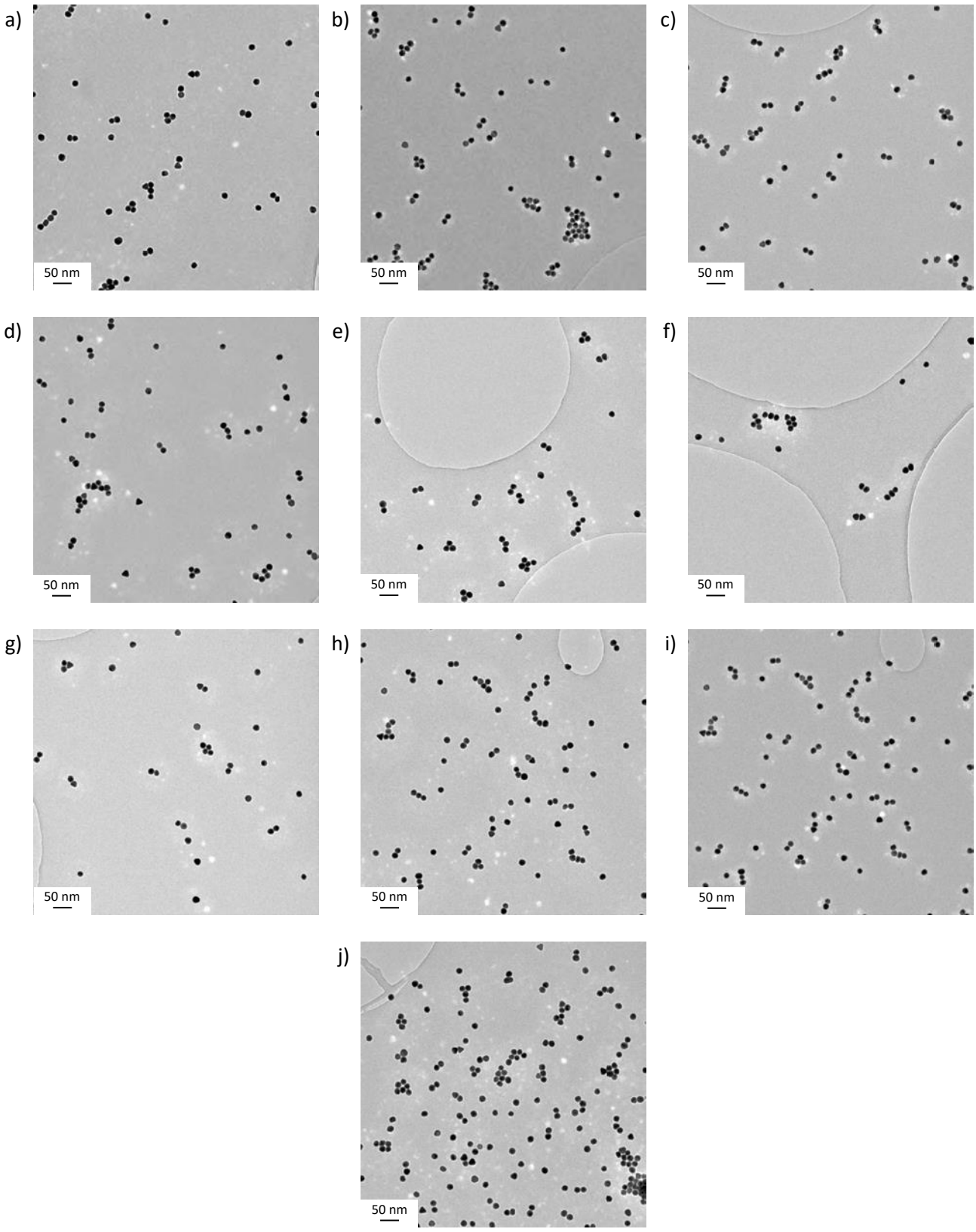

Figure S17 TEM images of the gold nanoparticle capped [2]rotaxane formed between 12 nm gold nanoparticles and CB[7]·**2**.

*CB[7]·**2** nanoparticle dimers purification:*

Direct implementation of the purification method reported by Akbulut *et al*.[8] for the dimer nanoparticle system formed between the 60 nm gold nanoparticles and the CB[7]·**2** complex was unsuccessful, because the dimer nanoparticle diameter (120 nm) is much bigger than the reference. However, we found that it is possible to purify the smaller nanoparticle dimers (Section S6.3) formed from the 12 nm gold nanoparticles with this method.

The citrate coated gold nanoparticles (12 nm) were used to obtain the nanoparticle dimers and purify it with a centrifugation method developed by Akbulut *et al*.[8] Three polymers (Brij, PEOE and Fricol) were mixed and centrifuged at 2000 rpm for 15 minutes, and then a concentrated gold nanoparticle solution (from 100 µL to 1 mL) was added carefully to the top of the polymer solution. The centrifugation was carried out for different times (1 min, 2 min, 3 min, 5 min, 7 min, and 9 min) where it showed that 6 minutes was the centrifugation time that yielded the best results. Different ratios of polymer and centrifugation speed have also been tested showing that the optimal conditions was 100 µL Brij, 200 µL PEOE, and 100 µL Fricol, 13000 rpm. The concentration of gold nanoparticle dimer was increased after purification and after repeating the purification process again, using the product of the first purification, a higher yield of the dimer was obtained where most of the product is dimer (~ 60 % dimers). Exposing the dimers to more than two purifications lead to inconsistent results. The resulting TEM images (Figure S18) shows that the ratio of dimers increased relatively, while the concentration of nanoparticles decreased after purification twice.

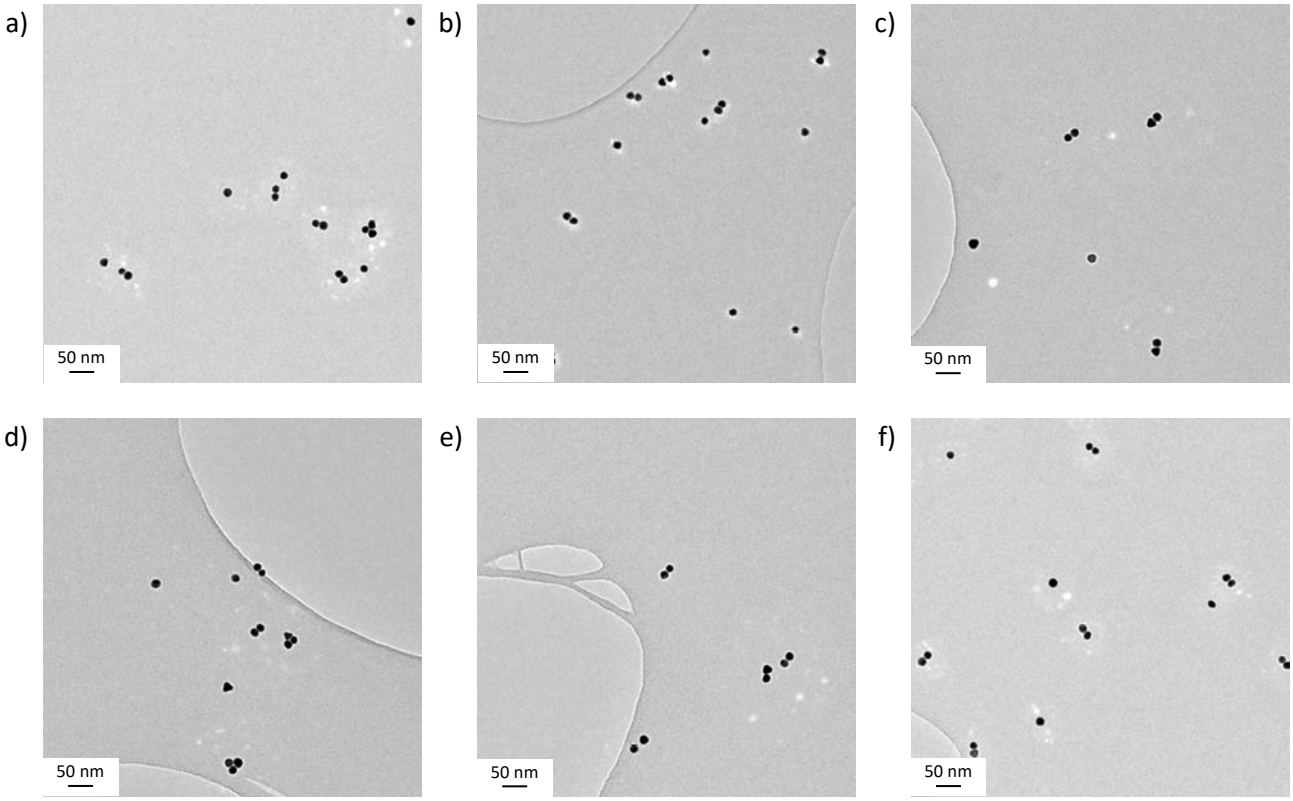

Figure S18 TEM images of the gold nanoparticle capped [2]rotaxane formed with an optimised synthetic procedure between 12 nm gold nanoparticles and CB[7]·**2**.

*Reference experiment, no CB[7]·**2** added to the gold nanoparticles:*

To confirm that the gold nanoparticle dimers are linked by the CB[7]·**2** complex a reference experiment without the CB[7] molecule linker was performed. Following the above described experimental procedure, without the addition of CB[7]·**2**, the gold nanoparticles (12 nm) are single dispersed and do not form dimers without the presence of CB[7]·**2** (Figure S19).

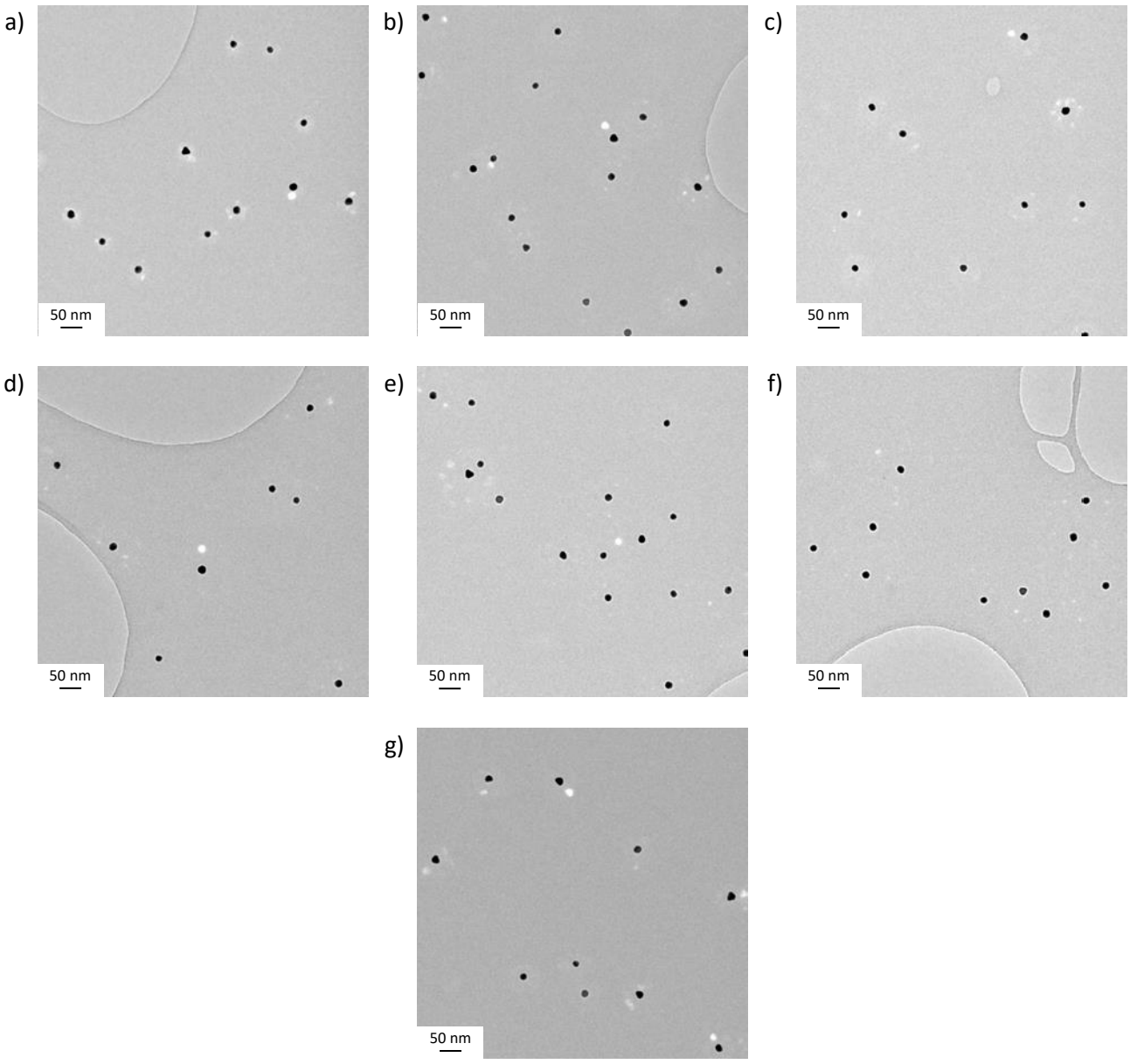

Figure S19 TEM images of the 12 nm gold nanoparticles without addition of CB[7]·**2**.

S7. NMR and MS spectra of synthesised compounds

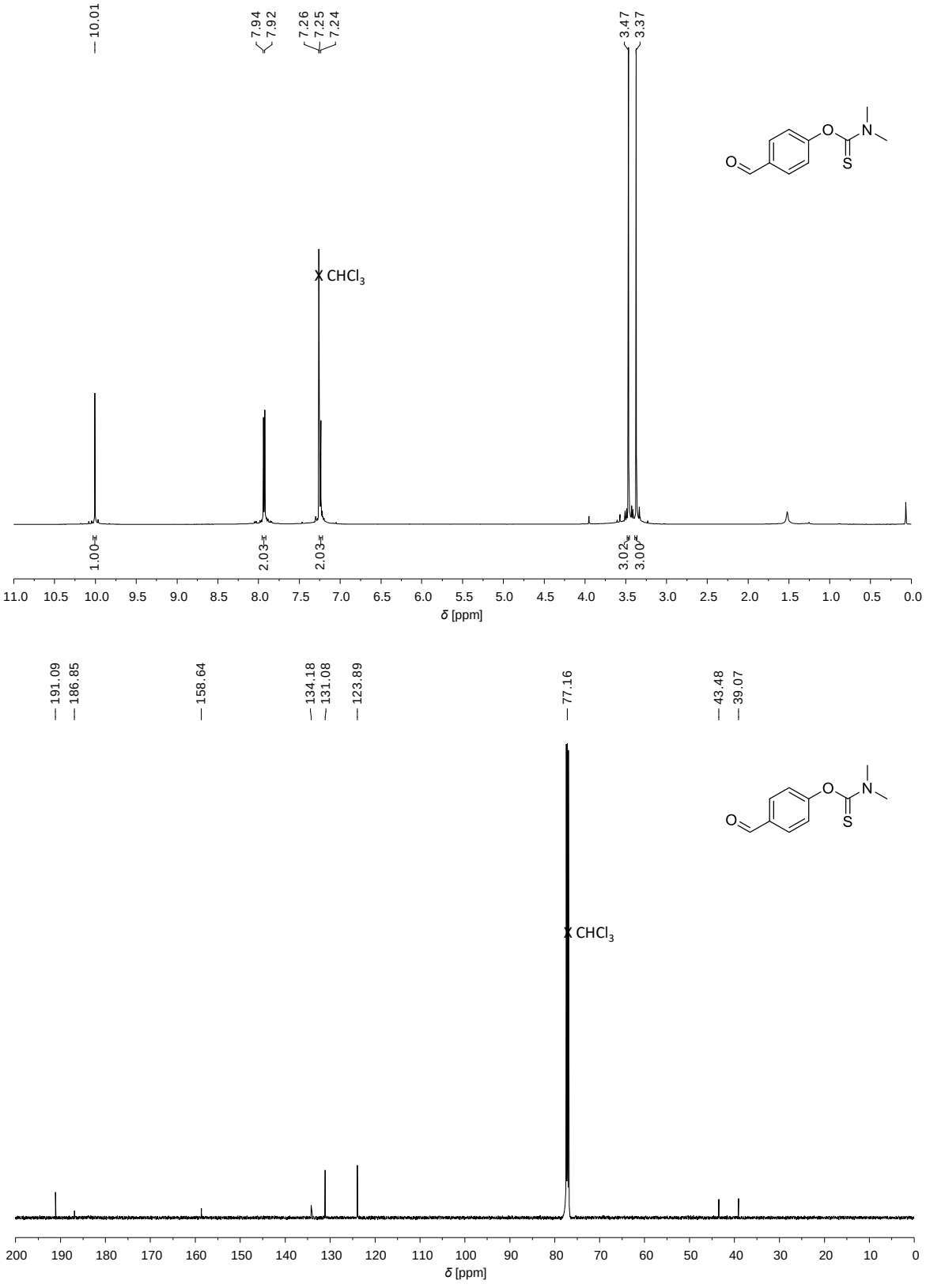

Figure S20 ^{1}H (top) and ^{13}C (bottom) NMR spectra of **S2** recorded in $CDCl_3$ at 25 °C.

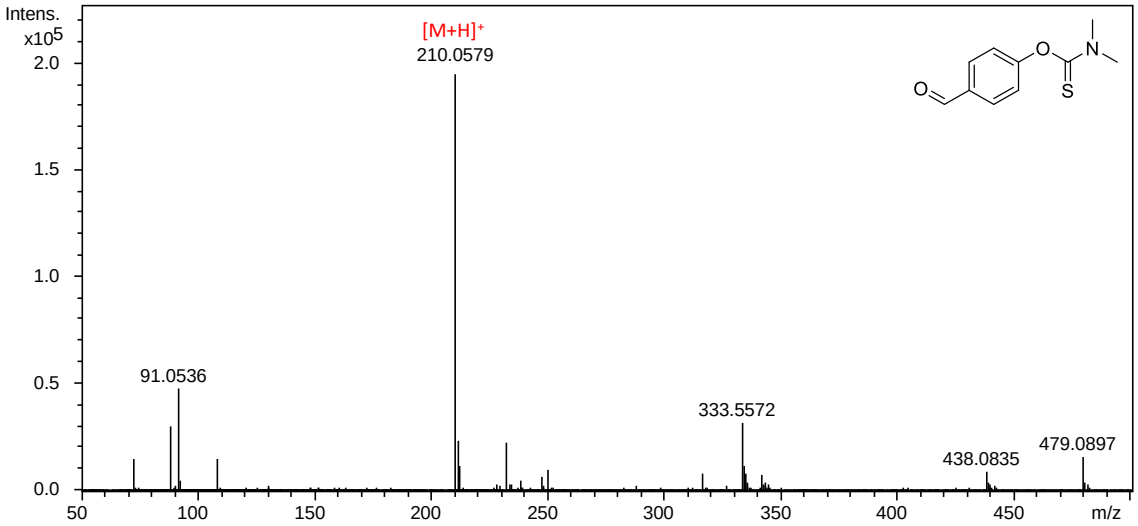

Figure S21 HR-ESI-TOF-MS spectrum of **S2**.

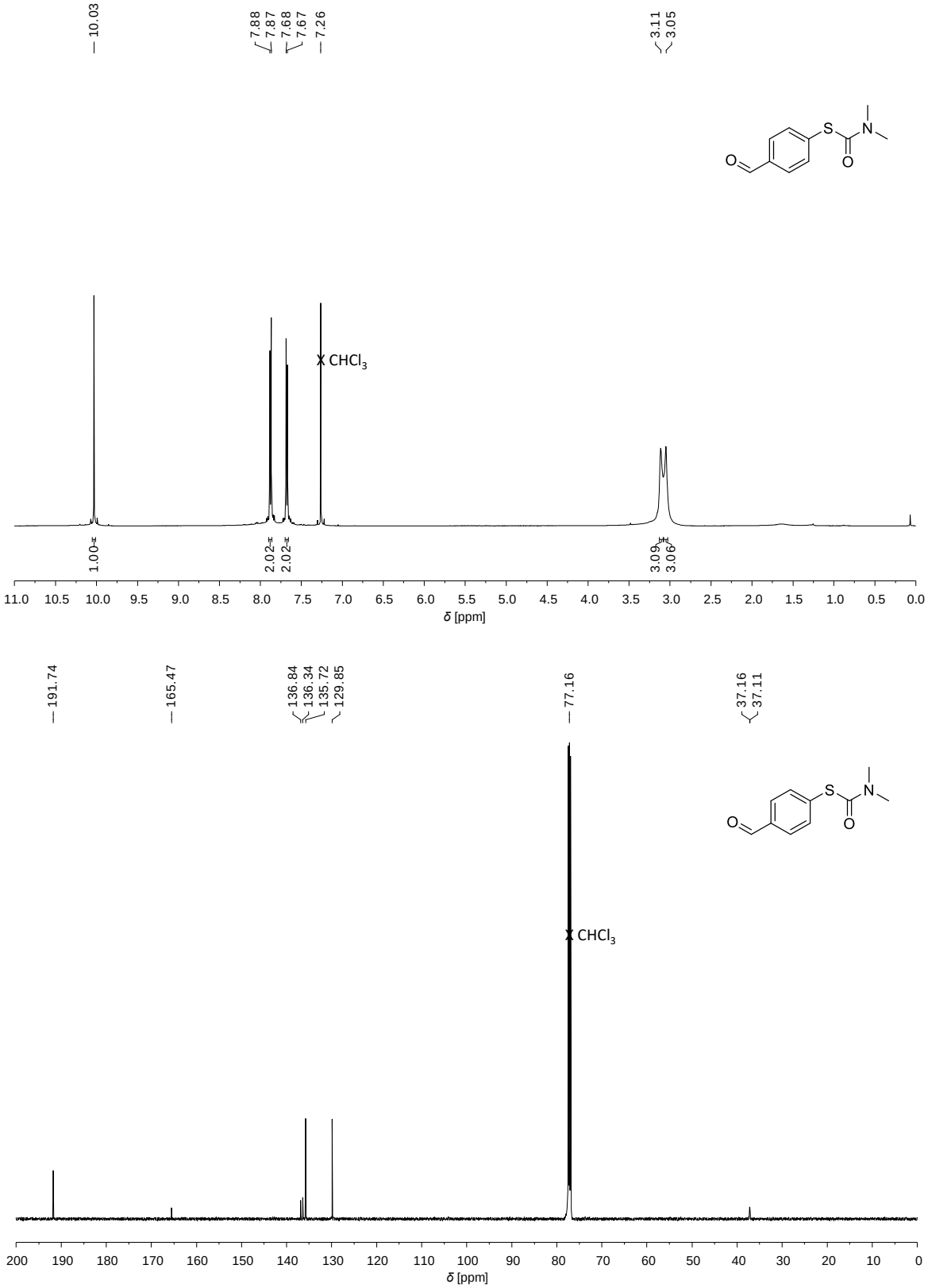

Figure S22 ^{1}H (top) and ^{13}C (bottom) NMR spectra of **S3** recorded in $CDCl_3$ at 25 °C.

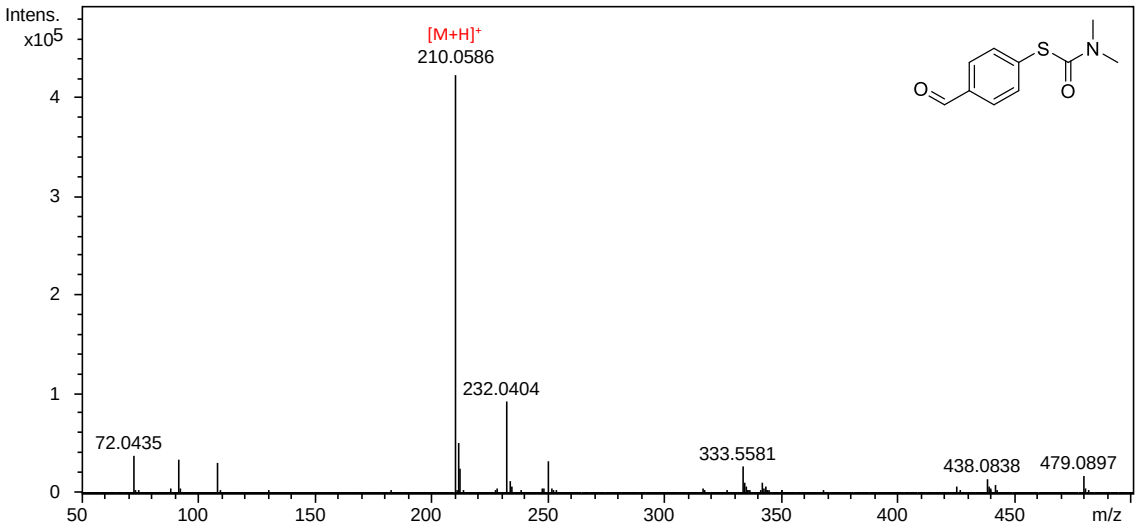

Figure S23 HR-ESI-TOF-MS spectrum of **S3**.

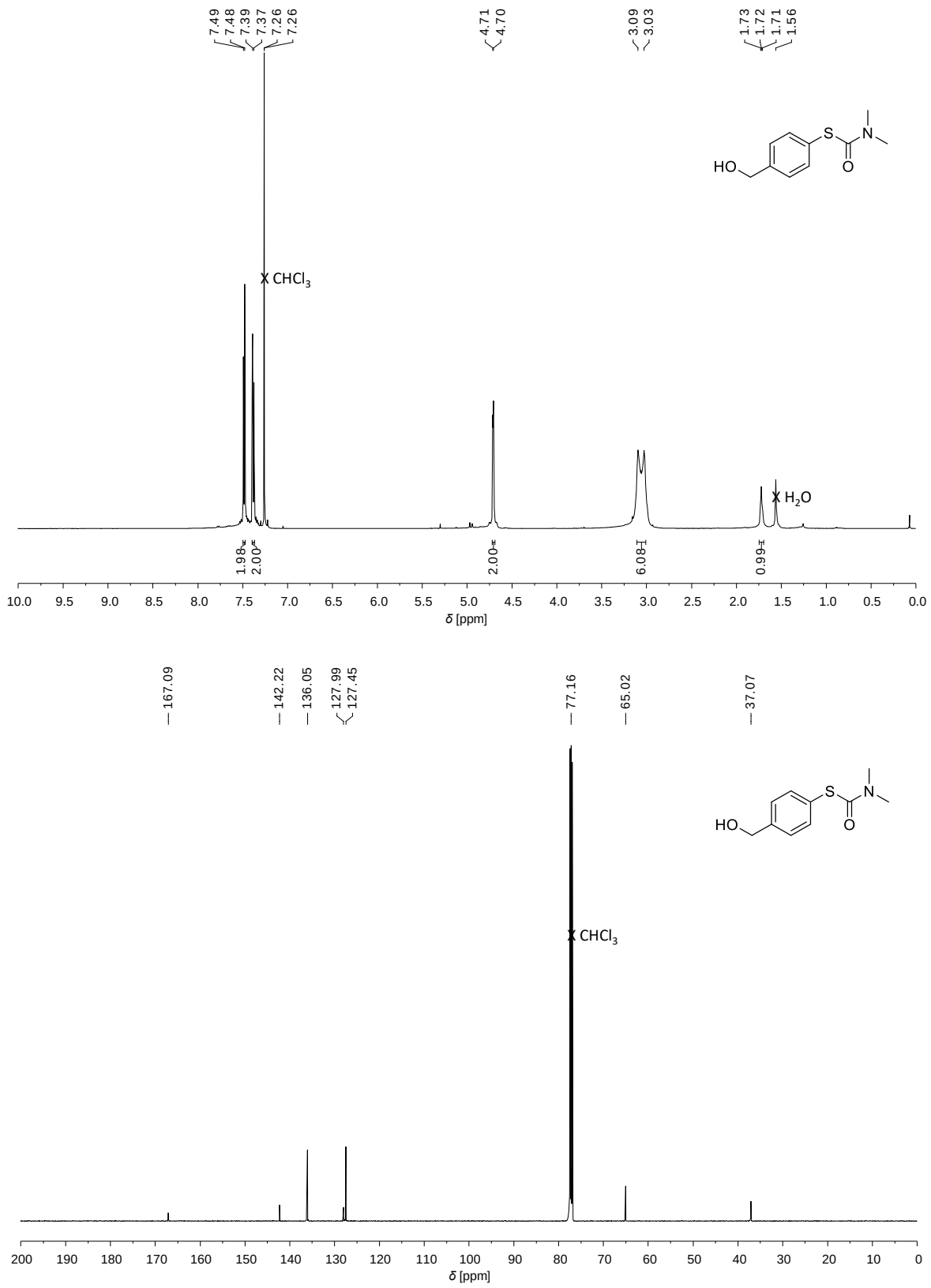

Figure S24 ^{1}H (top) and ^{13}C (bottom) NMR spectra of **S4** recorded in $CDCl_3$ at 25 °C.

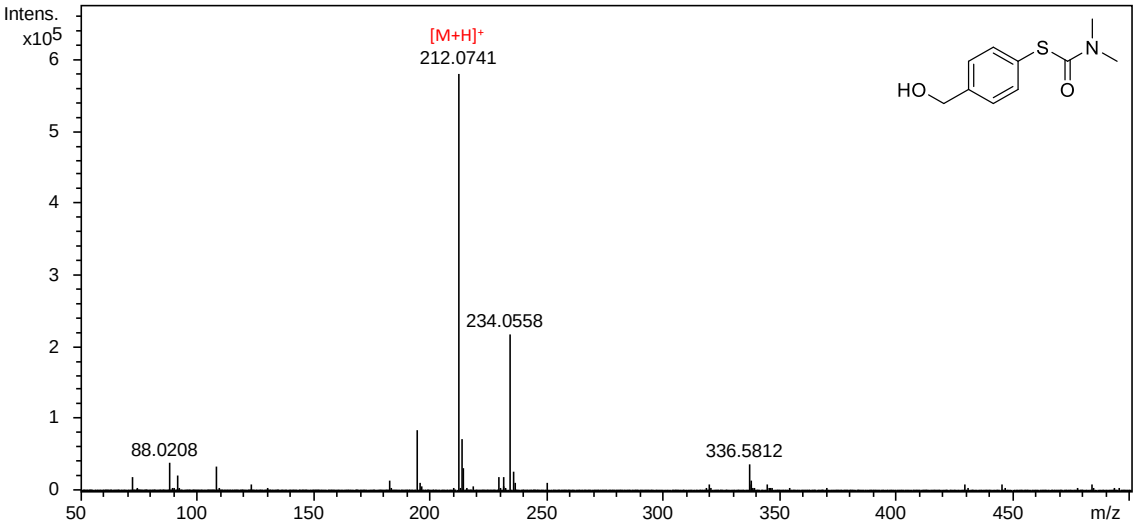

Figure S25 HR-ESI-TOF-MS spectrum of **S4**.

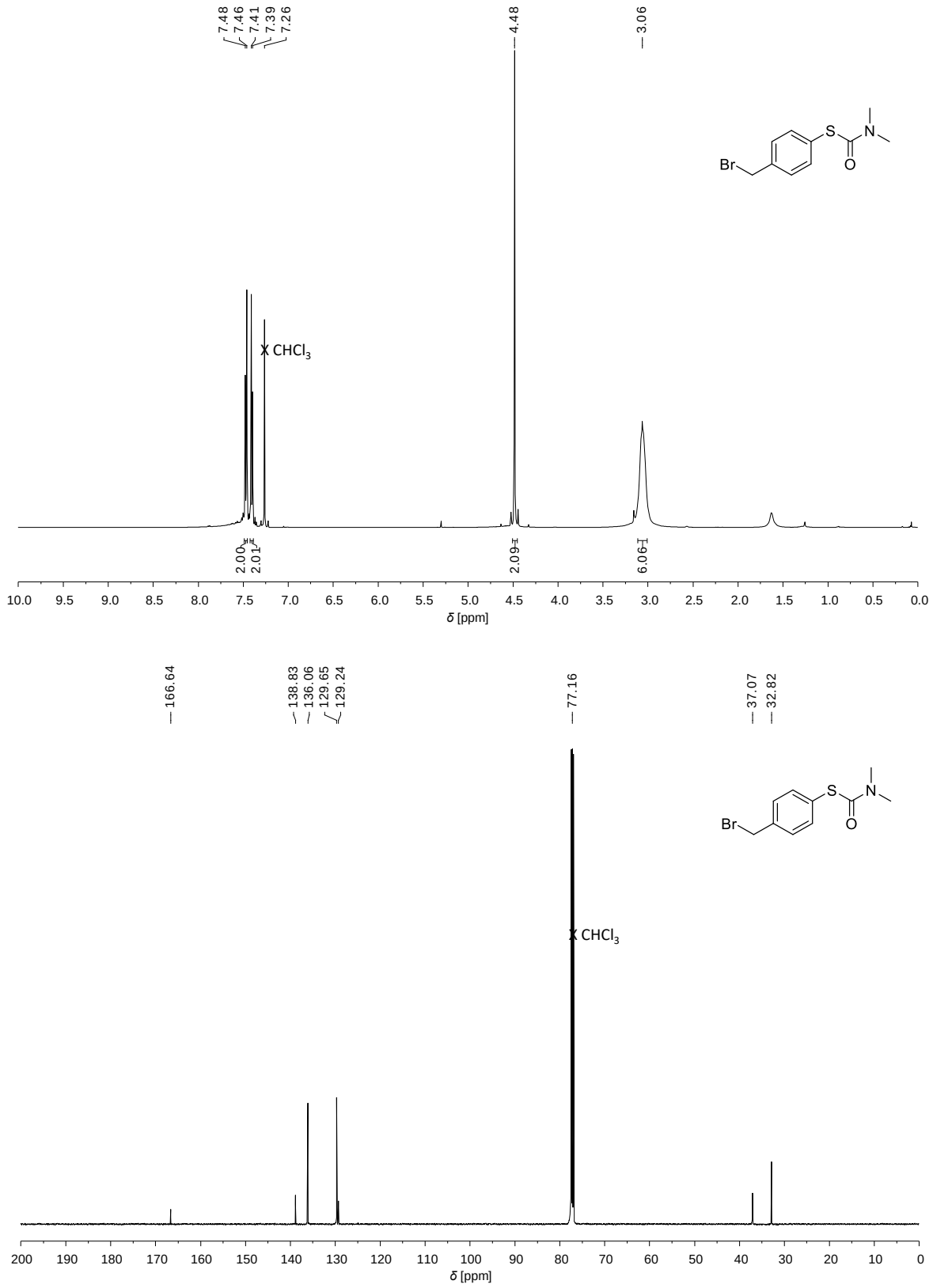

Figure S26 ^{1}H (top) and ^{13}C (bottom) NMR spectra of **S5** recorded in $CDCl_3$ at 25 °C.

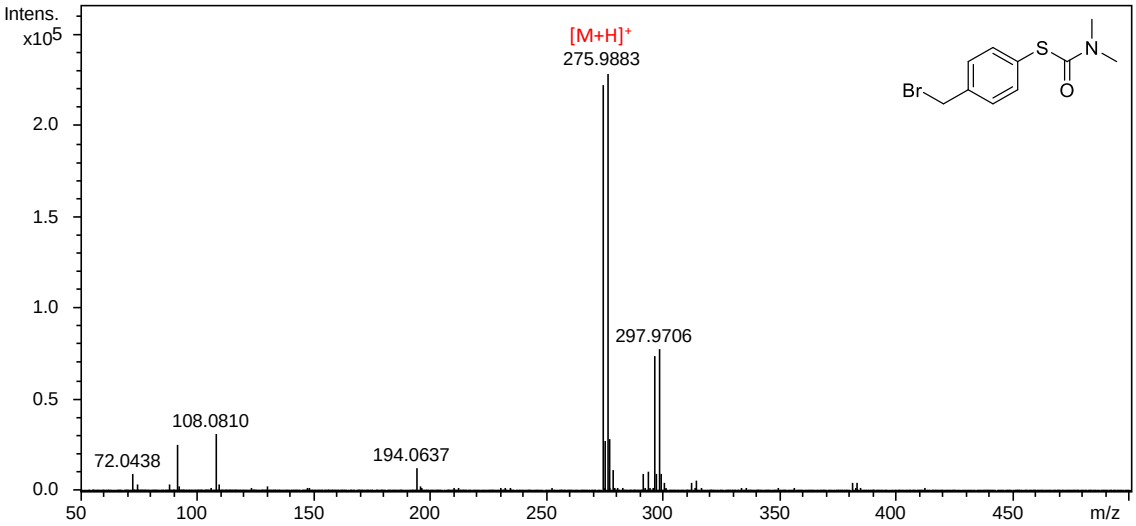

Figure S27 HR-ESI-TOF-MS spectrum of **S5**.

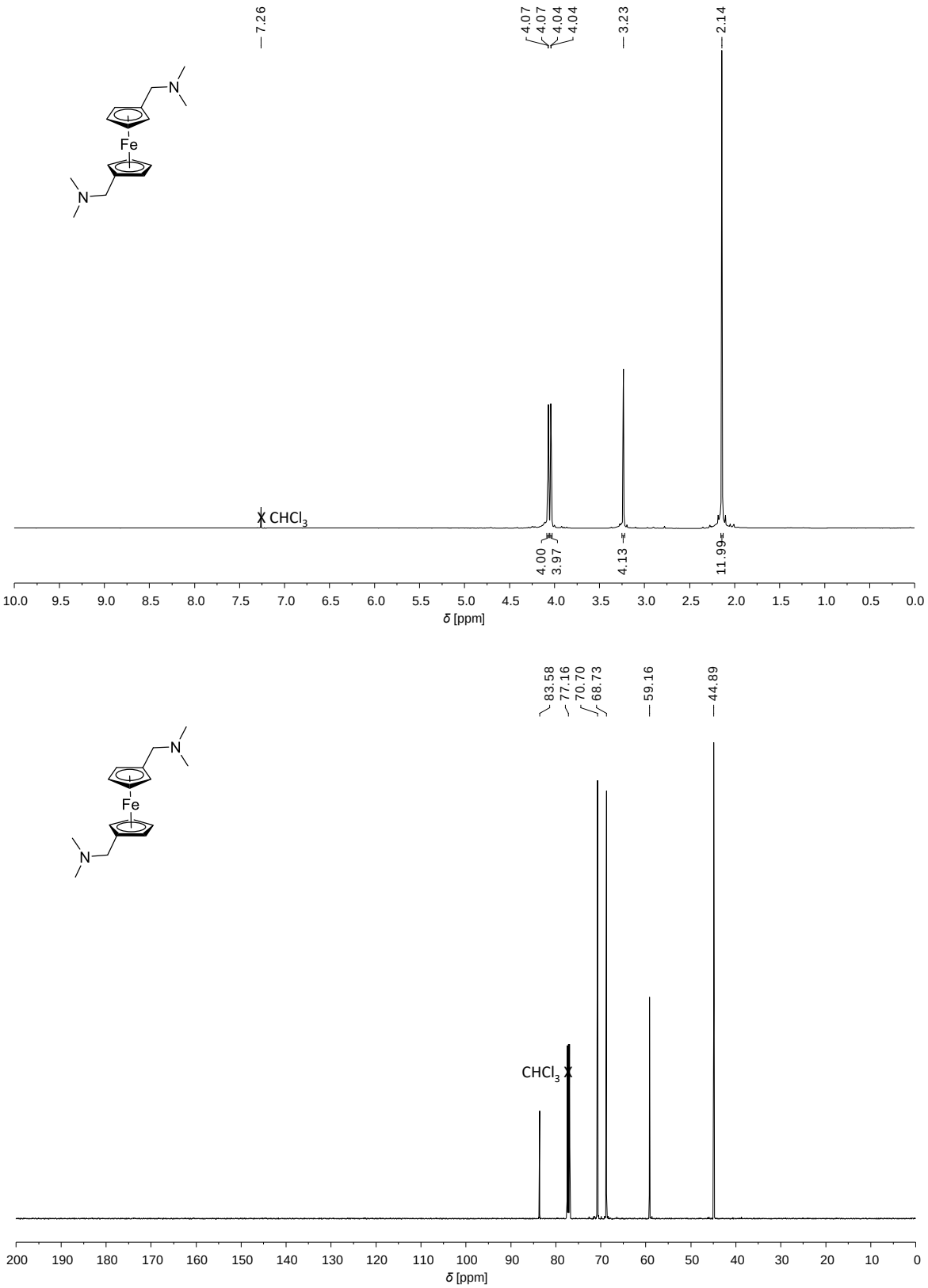

Figure S28 ^{1}H (top) and ^{13}C (bottom) NMR spectra of **S7** recorded in $CDCl_3$ at 25 °C.

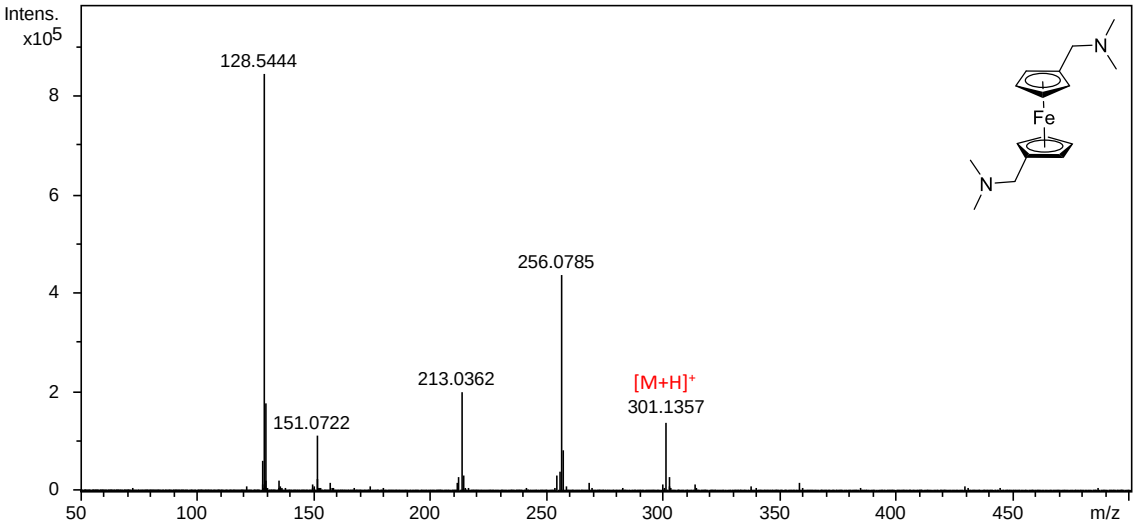

Figure S29 HR-ESI-TOF-MS spectrum of **S7**.

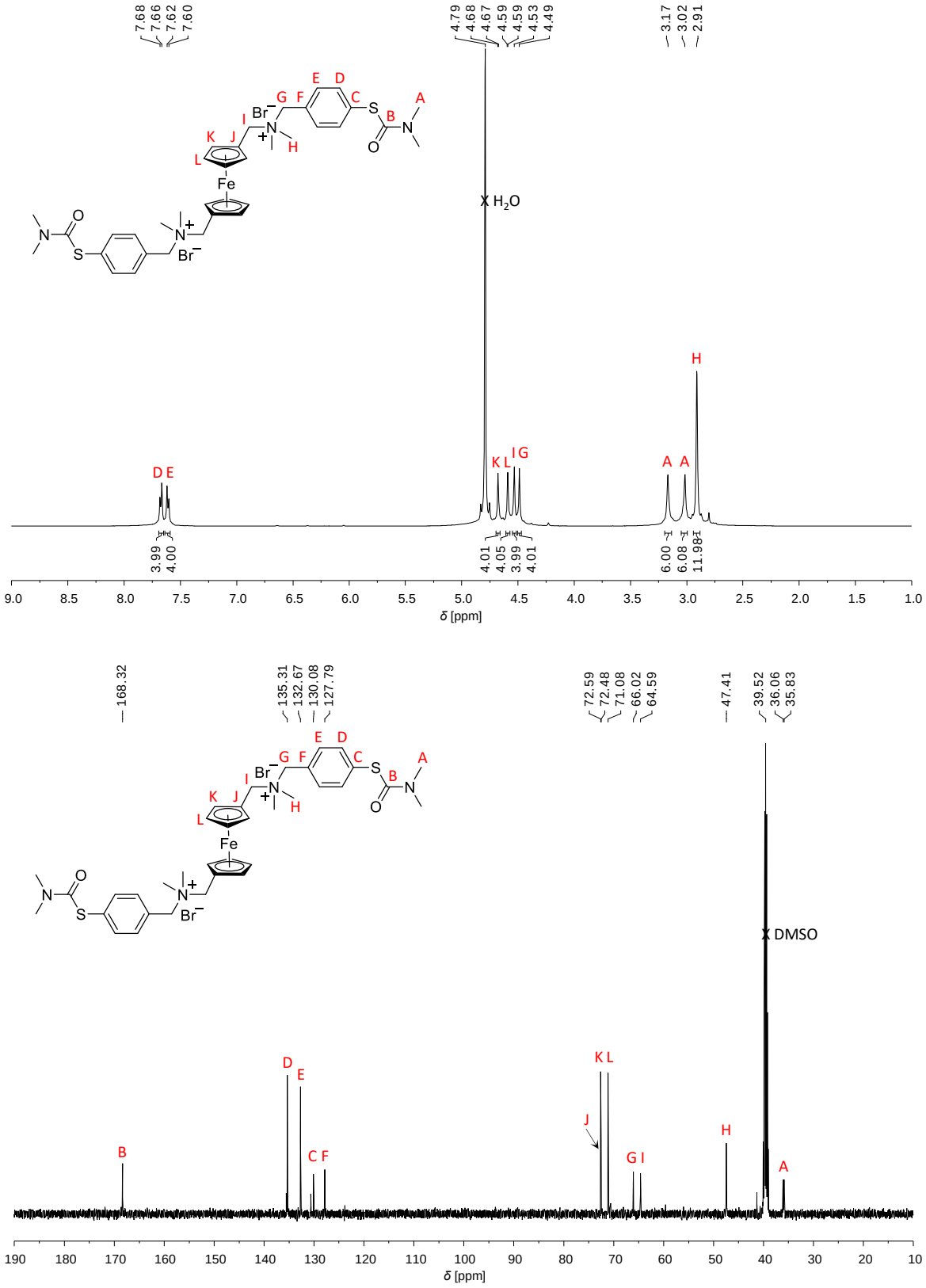

Figure S30 ^{1}H NMR spectrum of guest **1** recorded in 100 mM KCl in D_2O at 25 °C (top) and ^{13}C NMR spectrum recorded in 100 mM KCl in D_2O added a DMSO lock tube at 25 °C (bottom).

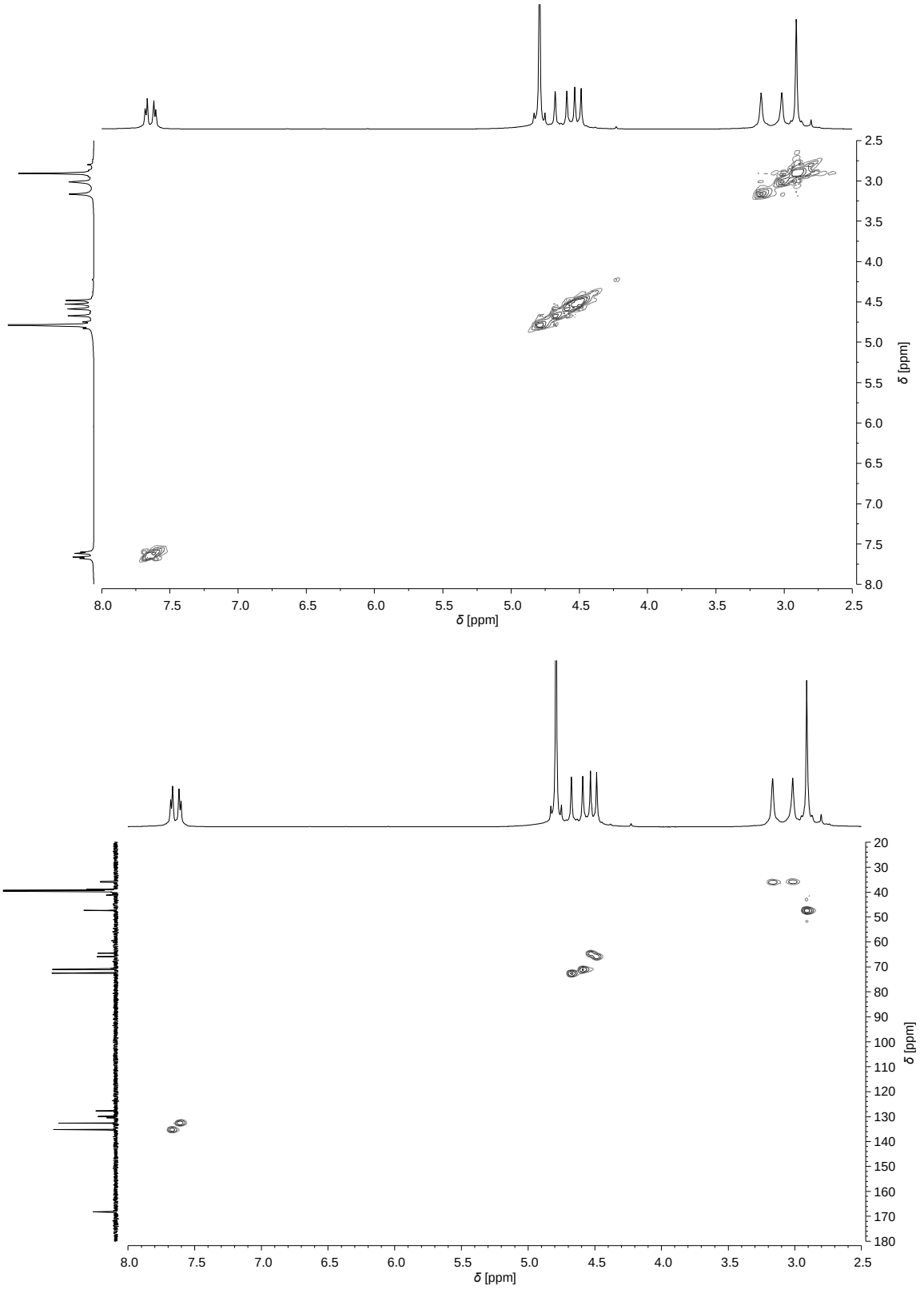

Figure S31 ^{1}H-^{1}H COSY (top) and ^{1}H-^{13}C HSQC (bottom) NMR spectra of guest **1** recorded in 100 mM KCl in D_2O added a DMSO lock tube at 25 °C.

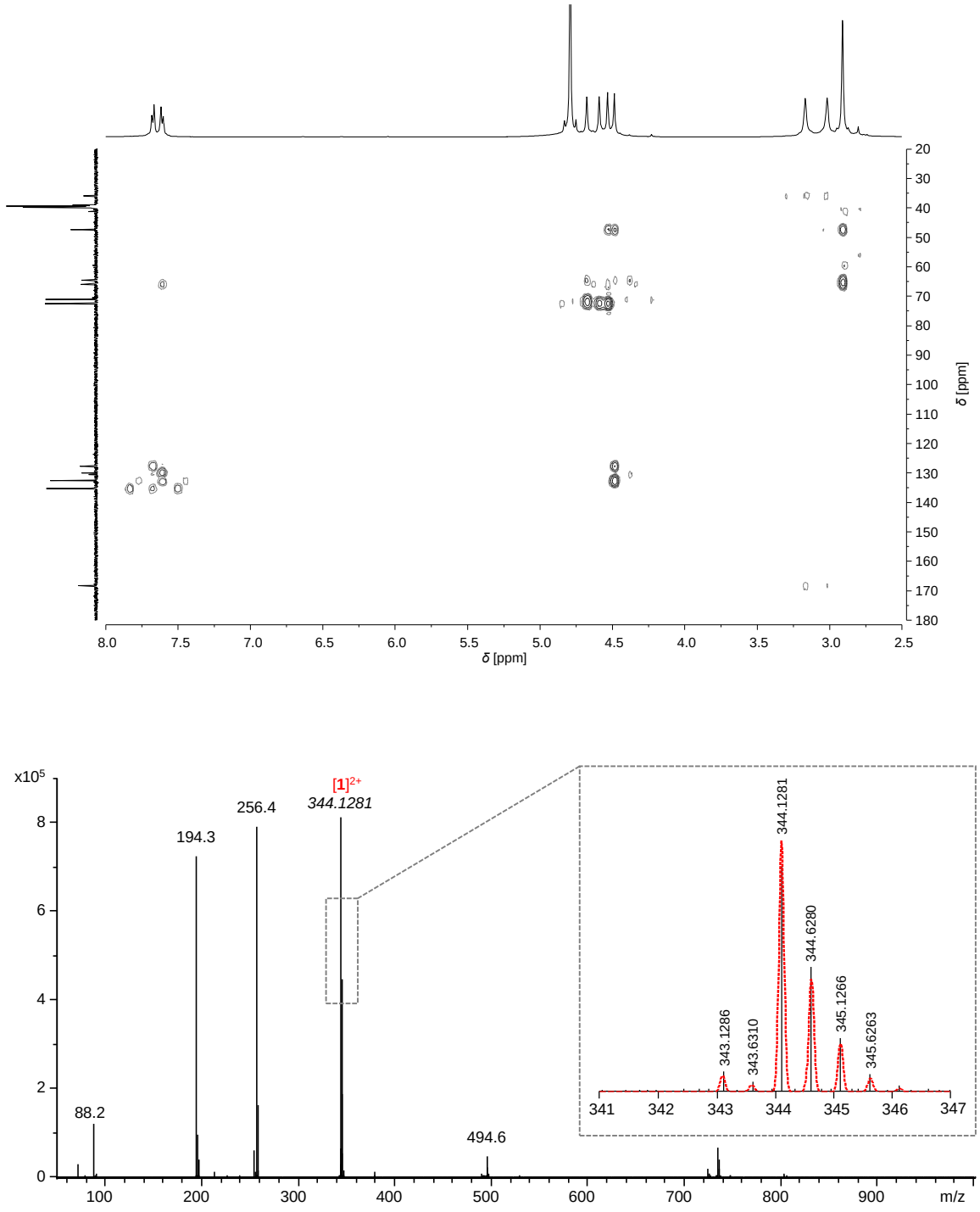

Figure S32 ^{1}H-^{13}C HMBC NMR spectrum of guest **1** recorded in 100 mM KCl in D_2O added a DMSO lock tube at 25 °C (top) and HR-ESI-TOF-MS spectrum of **1** (bottom). The insert shows a zoom of the isotopic distribution of the main peak where the calculated isotopic distribution is shown as red dotted lines while the black lines are the measured spectrum.

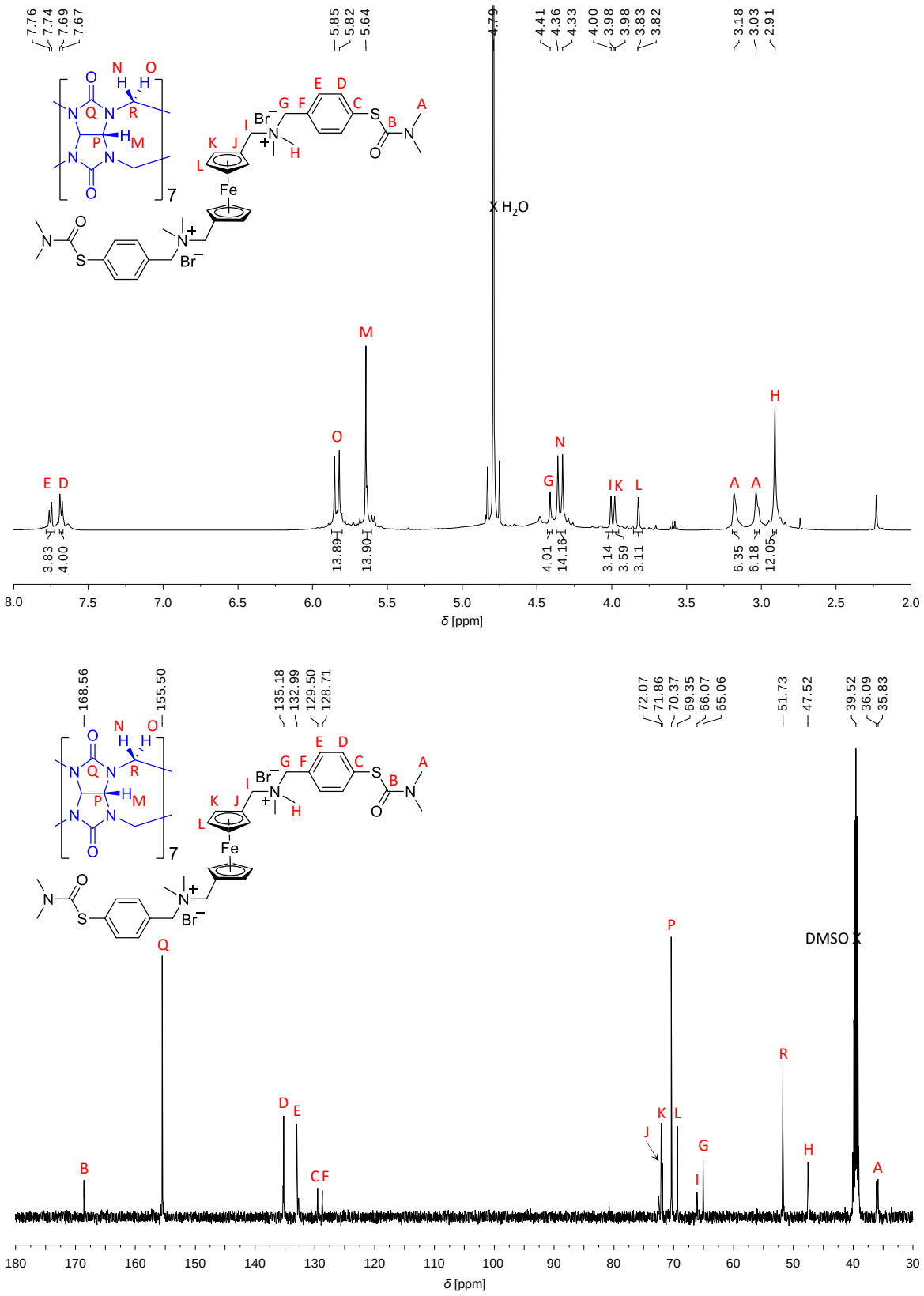

Figure S33 ^{1}H NMR spectrum of inclusion complex CB[7]·**1** recorded in 100 mM KCl in D_2O at 25 °C (top) and ^{13}C NMR spectrum recorded in 100 mM KCl in D_2O added a DMSO lock tube at 25 °C (bottom).

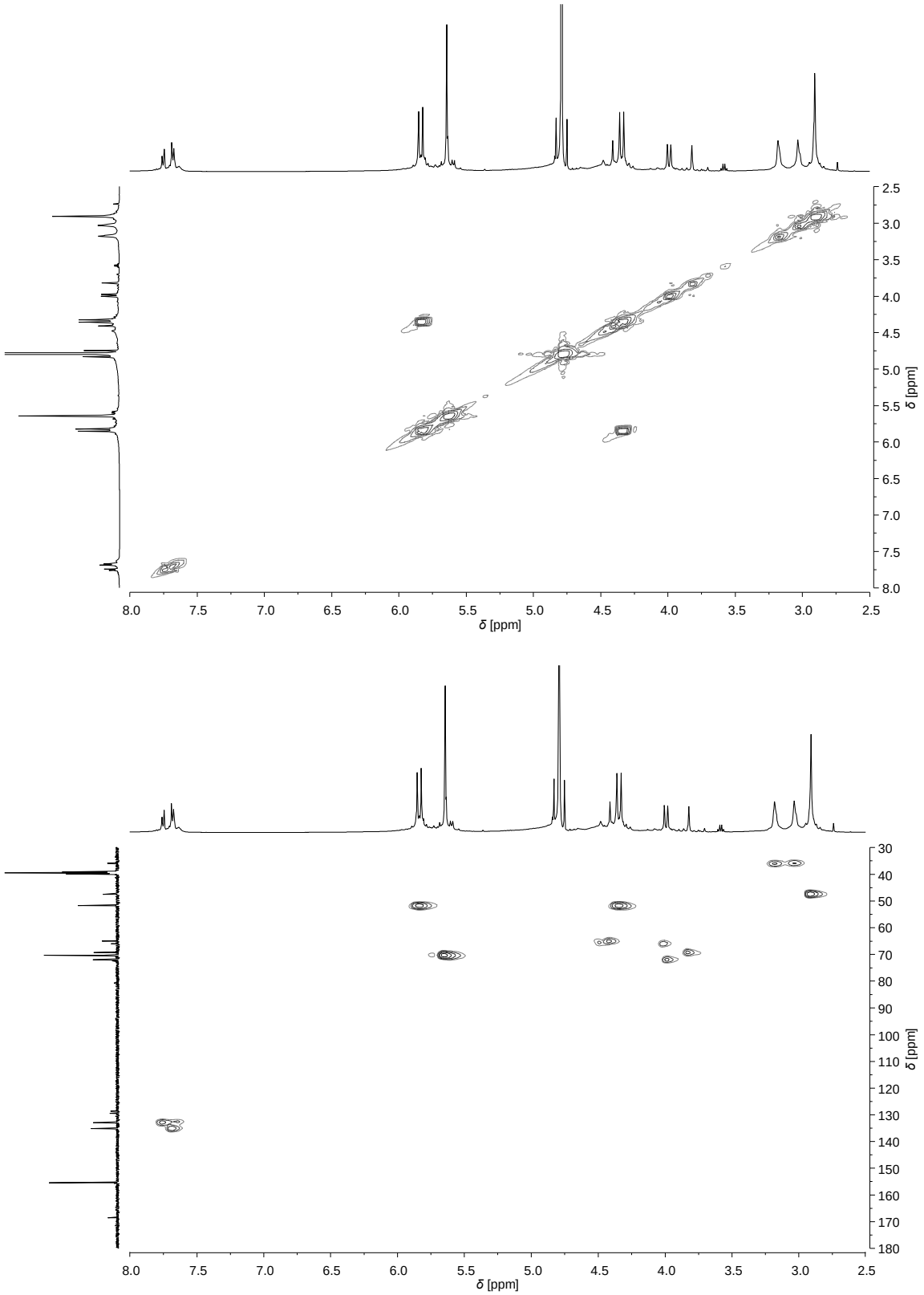

Figure S34 ^{1}H-^{1}H COSY (top) and ^{1}H-^{13}C HSQC (bottom) NMR spectra of inclusion complex CB[7]·**1** recorded in 100 mM KCl in D_2O added a DMSO lock tube at 25 °C.

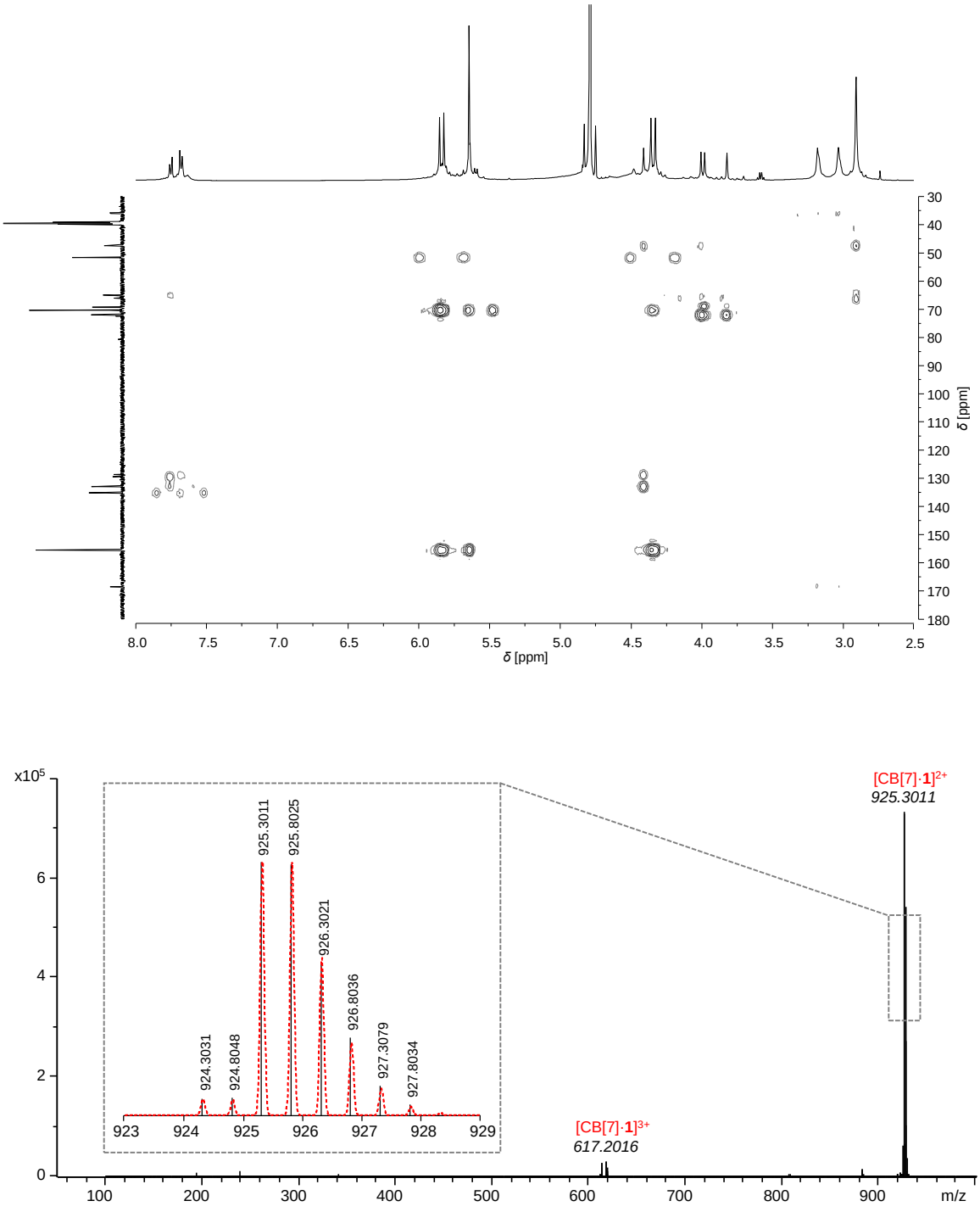

Figure S35 ^{1}H-^{13}C HMBC NMR spectrum of inclusion complex CB[7]·**1** recorded in 100 mM KCl in D_2O added a DMSO lock tube at 25 °C (top) and HR-ESI-TOF-MS spectrum of CB[7]·**1** (bottom). The insert shows a zoom of the isotopic distribution of the main peak where the calculated isotopic distribution is shown as red dotted lines while the black lines are the measured spectrum.

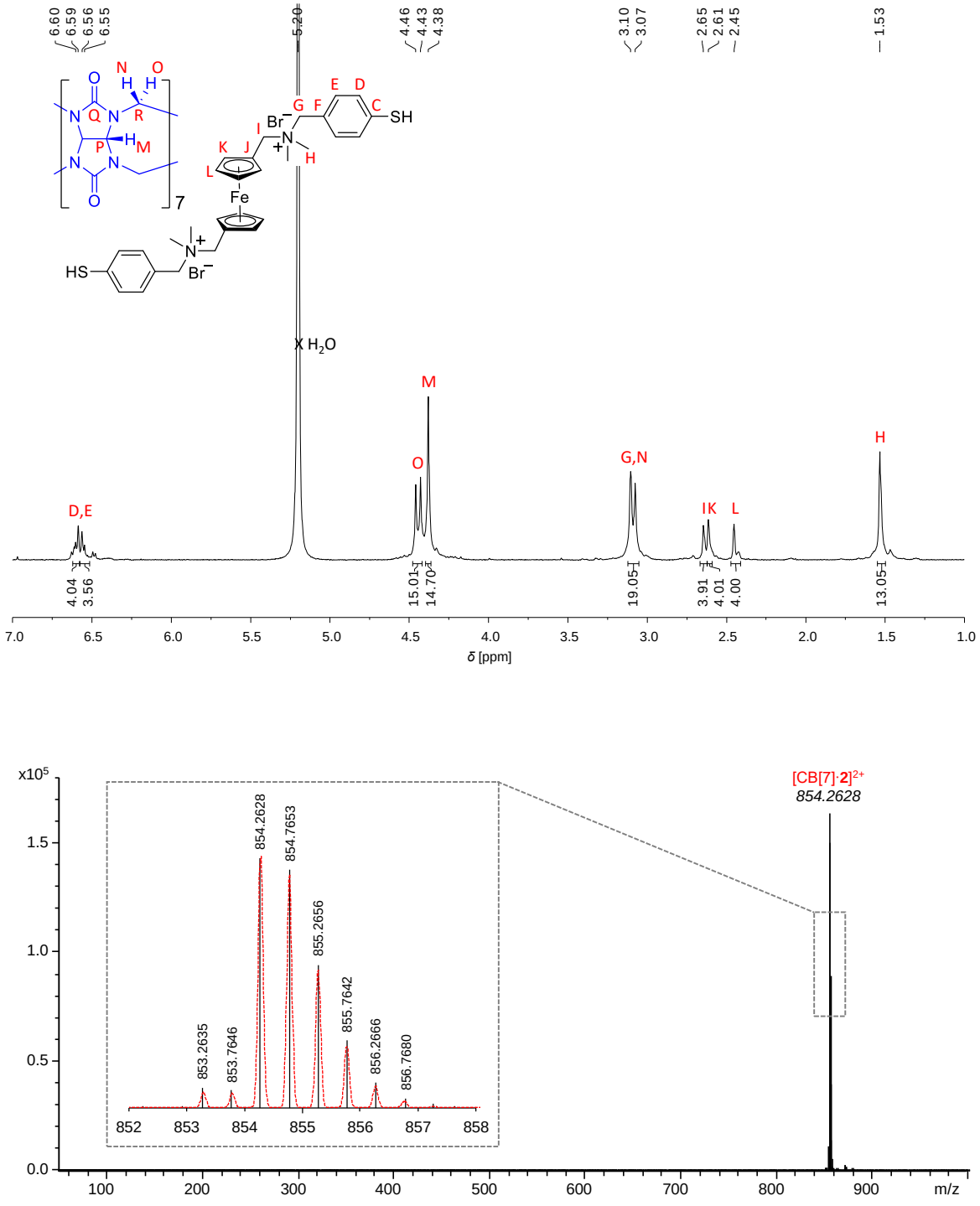

Figure S36 ^{1}H NMR spectrum of inclusion complex CB[7]·**2** recorded in 100 mM KCl in 4 M $DCl_{(aq)}$ at 25 °C (top) and HR-ESI-TOF-MS spectrum of CB[7]·**2** (bottom). The insert shows a zoom of the isotopic distribution of the main peak where the calculated isotopic distribution is shown as red dotted lines while the black lines are the measured spectrum.

S8. References

1. Glidewell, C.; Royles, B. J. L.; Smith, D. M., A simple high-yielding synthesis of ferrocene-1,'-diylbis-(methyltrimethylammonium iodide). *J. Organomet. Chem.* **1997,** *527* (1–2), 259-261.

2. Cao, L.; Šekutor, M.; Zavalij, P. Y.; Mlinarić-Majerski, K.; Glaser, R.; Isaacs, L., Cucurbit[7]uril·Guest Pair with an Attomolar Dissociation Constant. *Angew. Chem. Int. Ed.* **2014,** *53* (4), 988-993.

3. Randles, J. E. B., A cathode ray polarograph. Part II.-The current-voltage curves. *Transactions of the Faraday Society* **1948,** *44* (0), 327-338.

4. Nicholson, R. S., Theory and Application of Cyclic Voltammetry for Measurement of Electrode Reaction Kinetics. *Anal. Chem.* **1965,** *37* (11), 1351-1355.

5. Laviron, E., General expression of the linear potential sweep voltammogram in the case of diffusionless electrochemical systems. *J. Electroanal. Chem. Int. Electrochem.* **1979,** *101* (1), 19-28.

6. Grabar, K. C.; Freeman, R. G.; Hommer, M. B.; Natan, M. J., Preparation and Characterization of Au Colloid Monolayers. *Anal. Chem.* **1995,** *67* (4), 735-743.

7. McFarland, A. D.; Haynes, C. L.; Mirkin, C. A.; Van Duyne, R. P.; Godwin, H. A., Color My Nanoworld. *J. Chem. Educ.* **2004,** *81* (4), 544A.

8. Akbulut, O.; Mace, C. R.; Martinez, R. V.; Kumar, A. A.; Nie, Z.; Patton, M. R.; Whitesides, G. M., Separation of Nanoparticles in Aqueous Multiphase Systems through Centrifugation. *Nano Lett.* **2012,** *12* (8), 4060-4064.